

Meltwater Runoff from Haig Glacier, Canadian Rocky Mountains, 2002-2013

Shawn J. Marshall

Department of Geography, University of Calgary
2500 University Dr NW, Calgary AB, T2N 1N4, Canada
Email: shawn.marshall@ucalgary.ca

ABSTRACT. Observations of high-elevation meteorological conditions, glacier mass balance, and glacier runoff are sparse in western Canada and the Canadian Rocky Mountains, leading to uncertainty about the importance of glaciers to regional water resources. This needs to be quantified so that the impacts of ongoing glacier recession can be evaluated with respect to alpine ecology, hydroelectric operations, and water resource management. I assess the seasonal evolution of glacier runoff in an alpine watershed on the continental divide in the Canadian Rocky Mountains. Analysis is based on meteorological, snowpack and surface energy balance data collected at Haig Glacier from 2002-2013. The study area is one of several glacierized headwaters catchments of the Bow River, which flows eastward to provide an important supply of water to the Canadian prairies. Annual specific discharge from snow- and ice-melt on Haig Glacier averaged 2350mm water equivalent (w.e.) from 2002-2013, with 42% of the runoff derived from melting of glacier ice and firn, i.e. water stored in the glacier reservoir. This is an order of magnitude greater than the annual specific discharge from non-glacierized parts of the Bow River basin. From 2002-2013, meltwater derived from the glacier storage was equivalent to 5-6% of the flow of the Bow River in Calgary in late summer and 2-3% of annual discharge. The basin is typical of most glacier-fed mountain rivers, where the modest and declining extent of glacierized area in the catchment limits the glacier contribution to annual runoff.

1. Introduction

Meltwater runoff from glacierized catchments is an interesting and poorly understood water resource. Glaciers provide a source of interannual stability in streamflow, supplementing snow melt and rainfall (e.g., Fountain and Tangborn, 1985). This is particularly significant in warm, dry years (i.e. drought conditions), when ice melt from glaciers provides the main source of surface runoff once seasonal snow is depleted (e.g., Hopkinson and Young, 1998). At the same time, glacier runoff presents an unreliable future due to glacier recession in most of the world's mountain regions (Meier et al., 2007; Radić and Hock, 2011).

There is considerable uncertainty concerning the importance of glacier runoff in different mountain regions of the world. As an example, recent literature reports glacier inputs of 2% (Jeelani et al., 2012) to 32% (Immerzeel et al., 2009) within the upper Indus River basin in the western Himalaya. In the Rio Santo watershed of the Cordillera Blanca, Peru, Mark and Seltzer (2003) estimate glacier contributions of up to 20% of annual discharge, exceeding 40% during the dry season. Based on historical streamflow analyses and hydrological modeling in the Cordillera Blanca, Baraer et al. (2012) report even larger glacier contributions in highly-glacierized watersheds: up to 30% and 60% of annual and dry-season flows, respectively. In the Canadian Rocky Mountains, hydrological modeling indicates glacier meltwater contributions of up to 80% of July to September (JAS) flows, depending on the extent of glacier cover in a basin (Comeau et al., 2009).

Different studies cannot be compared, as the extent of glacier runoff depends on the time of year and the proportion of upstream glacier cover. Close to the glacier source (i.e. for low-order alpine streams draining glacierized valleys), glacial inputs approach 100% in late summer or in

the dry season. Further downstream, distributed rainfall and snowmelt inputs accrue, often filtered through the groundwater system, such that glacier inputs diminish in importance. Glacier runoff also varies over the course of the year, interannually, and over longer periods (i.e. decades) as a result of changing glacier area, further limiting comparison between studies.

Confusion also arises from ambiguous terminology; glacier runoff sometimes refers to meltwater derived from glacier ice, and sometimes to all water that drains off a glacier, including both rainfall and meltwater derived from the seasonal snowpack (e.g., Comeau et al., 2009; Nolin et al., 2010). The distinction is important because the seasonal snowpack on glaciers is ‘renewable’ – it will persist (although in altered form) in the absence of glacier cover. In contrast, glacier ice and firn serve as water reservoirs that are available as a result of accumulation of snowfall over decades to centuries. This storage is being depleted in recent decades, which eventually leads to declines in streamflow (Moore et al., 2009; Baraer et al., 2012). Glaciers are also intrinsically renewable, but sustained multi-decadal cooling is needed to build up the glacier reservoir, i.e. something akin to the Little Ice Age. In that sense, glaciers are similar to groundwater aquifers; depleted aquifers can recover, but not necessarily on time scales of relevance to societal water resource demands (Radic and Hock, 2014).

The importance of glaciers to surface runoff derived from the Canadian Rocky Mountains is also unclear. Various estimates of glacial runoff are available for the region, based largely on modeling studies and glacier mass balance measurements at Peyto Glacier (Hopkinson and Young, 1998; Comeau et al., 2009; Marshall et al., 2011), but there is little direct data concerning glacier inputs to streamflow for the many significant rivers that drain east, west, and north from the continental divide. This manuscript presents observations and modeling of glacier

runoff from a 12-year study on Haig Glacier in the Canadian Rocky Mountains, with the following objectives: (i) quantification of daily and seasonal meltwater discharge from the glacier, (ii) separation of runoff derived from the seasonal snowpack and that derived from the glacier ice reservoir, and (iii) evaluation of glaciers as landscape elements or hydrological ‘response units’ within the broader scale of watersheds in the Canadian Rocky Mountains.

Haig Glacier is one of several glacierized headwaters catchments that feed the Bow River, which drains eastward into the Canadian prairies. The Bow River is a modest but important drainage system that serves several population centres in southern Alberta, with a mean annual naturalized flow of $88 \text{ m}^3 \text{ s}^{-1}$ (specific discharge of 350 mm y^{-1}) at Calgary from 1972-2001 (Alberta Environment, 2004). The Bow River is heavily subscribed for agricultural and municipal water demands, and water withdrawal allocations from the river were frozen in 2006.

Source waters in the Rocky Mountains need to be better understood and quantified for water resource management in the basin, particularly in light of increasing population stress combined with the risk of declining summer flows in a warmer climate (Schindler and Donahue, 2006).

Based on relatively simple models, glacier storage inputs (ice and firn melt) for the period 2000-2009 have been estimated to constitute about 2% and 6% of annual and JAS flow of the Bow River in Calgary (Comeau et al., 2009; Marshall et al., 2011; Bash and Marshall, 2014).

Glacial inputs are therefore relatively unimportant in the downstream water budget for the basin, relative to contributions from rainfall and the seasonal mountain snowpack. They are likely to be in decline, however, given persistently negative glacier mass balance in the region over the last four decades and associated reductions in glacier area (Demuth et al., 2008; Bolch et al., 2010).

This may impact on the available water supply in late summer of drought years, when flows may

not be adequate to meet high municipal, agricultural, and in-stream ecological water demands. Moreover, glacier runoff during warm, dry summers can be significant in the Bow River (Hopkinson and Young, 1998), when demand is high and inputs from rainfall and seasonal snow are scarce. Glacier runoff has also been reported to be important in glacier-fed basins with limited glacier extent in the European Alps, e.g., more than 20% of August flow of the lower Rhone and Po Rivers (Huss et al., 2011).

The analysis presented here contributes observationally-based estimates of glacial runoff that can be used to improve modeling efforts, to understand long-term discharge trends in glacially-fed rivers (Rood et al., 2005; Schindler and Donahue, 2006), and to inform regional water resource management strategies. Sections 2 and 3 provide further details on the field site and glaciometeorological observations for the period 2002-2013, which are used to force a distributed energy balance and melt model for Haig Glacier. Section 4 summarizes the meteorological regime and provides estimates of glacier mass balance and meltwater runoff from the site, and Sections 5 and 6 discuss the main hydrological results and implications.

2. Study Site and Instrumentation

2.1 Regional Setting

Glaciological and meteorological studies were established at Haig Glacier in the Canadian Rocky Mountains in August 2000. Haig Glacier (50°43'N, 115°18'W) is the largest outlet of a 3.3-km² icefield that straddles the North American continental divide. The glacier flows to the southeast into the province of Alberta, with a central flowline length of 2.7 km (Figure 1). Elevations on the glacier range from 2435 to 2960 m, with a median elevation of 2662 m. There is

straightforward access on foot or by ski, enabling year-round study of glaciological, meteorological, and hydrological conditions (Shea et al., 2005; Adhikari and Marshall, 2013).

The eastern slopes of the Canadian Rocky Mountains are in a continental climate, with mild summers and cold winters. However, snow accumulation along the continental divide is heavily influenced by moist Pacific air masses. Persistent westerly flow combines with orographic uplift on the western flanks of the Rocky Mountains to give frequent winter precipitation events, associated with storm tracks along the polar front (Sinclair and Marshall, 2009). This combination of mixed continental and maritime influences gives extensive glaciation along the continental divide in the Canadian Rockies, with glaciers at elevations from 2200-3500 m on the eastern slopes.

The snow accumulation season in the Canadian Rockies extends from October to May, though snowfall occurs in all months. The summer melt season runs from May through September. Winter snow accumulation totals from 2002-2013 averaged 1700 mm w.e. at the continental divide location at the head of Haig Glacier (results presented below). For comparison, October to May precipitation in Calgary, situated about 100 km east of the field site, averaged 176 mm from 2002-2013 (Environment Canada, 2014), roughly 10% of the precipitation received at the continental divide.

2.2 Winter Mass Balance

This study focuses on summer melt modeling at Haig Glacier, with the winter snowpack taken as an ‘input’ or initial condition. Winter snowpack data used to initiate the model are based on annual snow surveys, typically carried out in the second week of May. Snow depth and density measurements are available from a transect of 33 sites along the glacier centreline (Figure 1),

with the sites revisited each spring. Snow pits are dug to the glacier surface at four sites, with density measurements at 10-cm intervals, and snow depths are attained by probing. Sites along the transect have a horizontal spacing of 50 m on the lower glacier (sites mb01-mb20) and 100 m on the upper glacier (mb21-mb33).

Snow survey data are available for the centreline transect for nine years from 2002-2013. For years without data, the mean snow distribution for the study period is assumed. Snowpack variability with elevation, $b_w(z)$, is fit with a polynomial function (Adhikari and Marshall, 2013). This function forms the basis for estimation of distributed snow depths and snow-water equivalence (SWE), $b_w(x,y)$. This treatment neglects lateral (cross-glacier) variability in the snowpack, introducing error to glacier-wide SWE estimates. Lateral snow-probing transects were carried out at three elevation bands in two years, to assess the error associated with cross-glacier variation in snow depths.

2.3 Meteorological Instrumentation

A Campbell Scientific automatic weather station (AWS) was set up on the glacier in the summer of 2001 (GAWS) and an additional AWS was installed in the glacier forefield in 2002 (FFAWS; Figure 1c). The weather stations are located at elevations of 2665 and 2340 m, respectively, and are 2.1 km apart. AWS instrumentation is detailed in Table 1. Station locations have been stable, but instruments are swapped out on occasion for replacement or calibration. From 2001-2008, the glacier AWS was drilled into the glacier and was raised or lowered through additional mainmast poles during routine maintenance every few months to keep pace with snow accumulation and melt. After 2008 the glacier AWS was installed on a tripod. The station blew over in winter

2012-2013 and was damaged beyond recovery due to snow burial and subsequent drowning during snowmelt in summer 2013; the last data download from the site was September 2012.

There are 2520 complete days (6.9 years) of observations from the GAWS from 2002-2012, of which 909 days are from June to August (JJA). This represents 90% coverage for the summer months (9.9 summers). Data is more complete from the FFAWS, with 3937 complete days of data (10.8 years) and 1004 days in JJA (10.9 summers) from 2002-2013. We visit the glacier year-round to service the weather stations, with a total of 67 visits from 2000-2013. The weather stations nevertheless fail on occasion due to power loss, snow burial, storm damage, excessive leaning, or, on two occasions, blow-down. Snow burial is problematic on the glacier in late winter, and in some years we opted for summer-only observations at the glacier site. This gives numerous data gaps at the GAWS, but there are sufficient data to examine year-round meteorological conditions.

Additional temperature-humidity (T - h) sensors, manufactured by Veriteq Instruments Inc., are installed year-round on the glacier and are raised or lowered on site visits to try and maintain a minimum measurement height of more than 50 cm above the glacier surface. Sensors are enclosed in radiation shields. These sites are mainly used to measure spatial temperature variability on the glacier, particularly near-surface temperature lapse rates. The Veriteq T - h transect is visited one to two times per year to download data and reset the loggers. Data are recorded at 30- or 60-minute intervals and represent snapshots rather than average conditions. During winter visits, sensors on the glacier are raised up through additional poles in order to remain above the snow, but winter burial occurred on numerous occasions, particularly on the upper glacier. In addition, there is occasional summer melt-out of poles that are drilled into the

glacier, resulting in toppled sensors. Instrument readings from fallen or buried sensors are easily detected from low temperature variability and high, constant humidity (typically 100%); all data from these periods ~~is~~ ^{are} removed from the analysis. Field calibrations indicate an accuracy of $\pm 0.4^{\circ}\text{C}$ for daily average temperatures with the Veriteq sensors.

2.4 Stream Data

Meltwater from Haig Glacier is drains through a combination of supraglacial streams and subglacial channels. The latter transport the bulk of the runoff, due to interception of surface drainage channels by moulins and crevasses. Meltwater is funneled into a waterfall in front of the glacier, and within about 500 m of the glacier terminus runoff is collected into a single, confined bedrock channel. This proglacial stream flows into the Upper Kananaskis River and goes on to feed the Kananaskis and Bow rivers in the Rocky Mountain foothills. Glacier runoff was measured in Haig Stream in 2002, 2003, 2013 and 2014, at a site about 900 m from the glacier terminus (Figure 1).

The stream-gauging site and general hydrometeorological relationships are described in Shea et al. (2005). In summer 2013, continuous pressure measurements in Haig Stream were conducted from late July until late September using a LevelTroll 2000. To establish a stream rating curve, discharge measurements were made using the velocity-profile method on three different visits from July through September, including bihourly measurements over a diurnal cycle to capture high and low flows.

The runoff data are limited, but provide insights into the nature and time scale of meltwater drainage from Haig Glacier. Shea et al. (2005) report delays in runoff of approximately 3 hours from peak glacier melt rates to peak discharge at Haig Stream during the late summer (July

through September). Delays are longer in May and June, when the glacier is still snow-covered, probably due to a combination of mechanisms (Willis et al., 2002): (i) the supraglacial snow cover acts effectively as an aquifer to store meltwater and retard its drainage, (ii) access to the main englacial drainage pathways, crevasses and moulins, is limited, and (iii) the subglacial drainage system (tunnel network) is not established. Some early-summer meltwater runs off, as the proglacial waterfall awakens and Haig Stream becomes established during May or June each year, initially as a sub-nival drainage channel. A portion of early-summer meltwater on the glacier may experience delays of weeks to months. We do not have good constraints on this.

3. Methods

Haig Glacier meltwater estimates in this paper are reported for 2002-2013, for which winter snowpack and meteorological data are available from the site. Meteorological and surface energy balance regimes are characterized at the GAWS site, and distributed energy balance and melt models are developed and forced using this data. This is common practice in glacier melt modeling (e.g., Arnold et al., 1996; Klok and Oerlemans, 2002; Hock and Holmgren, 2005), although simplified temperature-index melt models are still widely-used where insufficient meteorological input data are available (e.g., Huss et al., 2008; Nolin et al., 2010; Immerzeel et al., 2013; Bash and Marshall, 2014).

Temperature-index melt models are more easily distributed than surface energy balance models and can perform better in the absence of local data (Hock, 2005). However, there are numerous reasons to develop and explore more detailed, physically-based energy balance models and to resolve daily energy balance cycles, particularly as interest grows in modeling of glacial runoff. Diurnal processes that affect seasonal runoff include overnight refreezing, which delays

meltwater production the following day, systematic differences in cloud cover through the day (e.g., cloudy conditions developing in the afternoon in summer months), diurnal development of the glacier boundary layer due to daytime heating, and storage/delay of meltwater runoff, which can be evaluated from diurnal hydrographs and their seasonal evolution. These processes are not the focus of this manuscript, but the model is being developed with such questions in mind, and the energy balance treatment described below will serve as a building block for followup studies.

3.1 Meteorological Forcing Data

Meteorological data from the GAWS are used to calculate surface energy balance at this site for the May through September (MJJAS) melt season. Daily mean conditions from 2002-2012 at the forefield and glacier AWS sites are also compiled to characterize the general meteorological regime. Relations between the two sites are used to fill in missing data from the GAWS site, following either $\beta_G = \beta_{FF} + \Delta\beta_d$ or $\beta_G = k_d\beta_{FF}$, where β is the variable of interest, $\Delta\beta_d$ is the mean daily offset between the glacier and forefield sites, and k_d is a scaling factor used where a multiplicative relation is appropriate for mapping forefield conditions onto the glacier. Values for $\Delta\beta_d$ and k_d are calculated from all available data for that day in the 11-year record.

Temperature, T , is modeled through an offset, while specific humidity, q_v , wind speed, v , and incoming solar radiation, Q_s^\downarrow , are scaled through factors k_d . A temperature offset is adopted to adjust the temperature rather than a lapse-rate correction because of the different surface energy conditions at the two sites during the summer. After melting of the seasonal snowpack at the FFAWS, typically during June, the exposed rock heats up in the sun and is not constrained to a surface temperature of 0°C, as is the glacier surface. Hence, summer temperature differences are much larger than annual mean differences between the sites. Other aspects of the energy balance

regime also differ (e.g., local radiative and advective heating in the forefield environment). Free-air or locally-determined near-surface lapse rates do not make sense in this situation, whereas temperature offsets capture the cooling influence of the glacier associated with differences in the surface energy balance, as well as differences due to elevation.

GAWS air pressure, p , is estimated from the forefield data through the hydrostatic equation, $\Delta p / \Delta z = -\rho_a g$, where Δz is the vertical offset between the AWS sites, g is gravity, and $\rho_a = (\rho_G + \rho_{FF})/2$ is the average air density between the sites. Air density is calculated from the ideal gas law at each site, $p = \rho_a R T$, for gas law constant R . Because this involves both pressure and density, air pressure and density are calculated iteratively.

Where neither GAWS nor FFAWS data are available, missing meteorological data are filled using mean values for that day. For energy balance and melt modeling, diurnal cycles of temperature and incoming solar radiation are important. Where GAWS data are available (90% of days for June-August (JJA) and 86% of days for May-September (MJJAS)), 30-minute temperature and radiation data resolve the daily cycle directly. Otherwise, a sinusoidal temperature cycle for temperature is adopted, using T_{Gs} along with the average measured daily temperature range, T_{rd} : $T_G(h) = T_{Gs} - T_{rd}/2 \cos(2\pi (t - \tau)/24)$, for hour $t \in (0, 24)$ and lag $\tau \sim 4$ hours. For incoming solar radiation, the diurnal cycle is approximated using a half-sinusoid with the integrated area under the curve equal to the total daily radiation Q_{sd}^\downarrow (in units of $\text{J m}^{-2} \text{d}^{-1}$). Wind conditions, specific humidity, and air pressure are assumed to be constant over the day when daily fields are used to drive the melt model.

3.2 Local Surface Energy Balance

Net surface energy, Q_N , is calculated from:

$$Q_N = Q_S^\downarrow - Q_S^\uparrow + Q_L^\downarrow - Q_L^\uparrow + Q_G + Q_H + Q_E, \quad (1)$$

in which Q_S^\downarrow is the incoming shortwave radiation at the surface, $Q_S^\uparrow = \alpha_s Q_S^\downarrow$ is the reflected shortwave radiation, for albedo α_s , Q_L^\downarrow and Q_L^\uparrow are the incoming and outgoing longwave radiation, Q_C is the subsurface energy flux associated with heat conduction in the snow/ice, Q_H and Q_E are the turbulent fluxes of sensible and latent heat, and heat advection by precipitation and runoff taken to be negligible. All energy fluxes have units W m^{-2} . By convention, Q_E refers only to the latent heat of evaporation and sublimation. Q_N represents the energy flux available for driving snow/ice temperature changes and for latent heat of melting and refreezing:

$$Q_N = \begin{cases} \rho_s L_f \dot{m}, & T_s = 0^\circ\text{C} \text{ and } Q_N \geq 0, \\ \rho_w L_f \dot{m}, & T_s = 0^\circ\text{C} \text{ and } Q_N < 0 \text{ and water available,} \\ \rho_s c_s d \frac{\partial T}{\partial t}, & T_s < 0^\circ\text{C} \text{ or } (T_s = 0^\circ\text{C}, Q_N < 0, \text{ no water}). \end{cases} \quad \begin{matrix} (2a) \\ (2b) \\ (2c) \end{matrix}$$

In general in the summer months, the glacier surface temperature, T_s , is at the melting point and melt rates, \dot{m} (m s^{-1}) are calculated following Eq. (2a), where ρ_s is the surface density (snow or ice density, with units kg m^{-3}) and L_f is the latent heat of fusion (J kg^{-1}). If net energy is negative, as it often is at night, available surface and near-surface water will refreeze, following Eq. (2b) with water density $\rho_w = 1000 \text{ kg m}^{-3}$. The final condition in Eq. (2c) refers to the change in internal energy of the near-surface snowpack or glacier ice if surface temperatures are below 0°C or if there is an energy deficit and no meltwater is available to refreeze. A near-surface layer of finite thickness d (m) warms or cools according to the specific heat capacity c_s ($\text{J kg}^{-1}^\circ\text{C}^{-1}$)

285 To evaluate the surface energy budget, the radiation terms are measured directly at the GAWS,
 286 while Q_C , Q_H , and Q_E are modeled. Q_C is modeled through one-dimensional (vertical) heat
 287 diffusion in a 50-layer, 10-m deep model of the near surface snow or ice, forced by air
 288 temperature at the surface-atmosphere interface and assuming isothermal (0°C) glacial ice
 289 underlying the surface layer. Meltwater is assumed to drain downward into the snowpack, and if
 290 the snowpack is below the melting point, meltwater will refreeze and release latent heat, which is
 291 introduced as an energy source term in the relevant layer of the snowpack model. The snow
 292 hydrology treatment is simplistic. An irreducible snow water content of 4% is assumed for the
 293 snowpack, based on the measurements of Coléou and Lesaffre (1998) and meltwater is assumed
 294 to percolate downwards into adjacent grid cells without delay. If the underlying grid cell is
 295 saturated, meltwater penetrates deeper until it reaches a grid cell with available pore space or it
 296 reaches the snow-ice interface. The glacier ice is assumed to be impermeable, with instantaneous
 297 runoff along the glacier surface.

298 Turbulent fluxes (W m^{-2}) are modeled through the standard profile method,

$$\begin{aligned}
 299 \quad Q_H &= \rho_a c_{pa} K_H \frac{\partial T_a}{\partial z} = \rho_a c_{pa} k^2 v \left[\frac{T_a(z) - T_a(z_{0H})}{\ln(z/z_0) \ln(z/z_{0H})} \right], \\
 Q_E &= \rho_a L_{s/v} K_E \frac{\partial q_v}{\partial z} = \rho_a L_{s/v} k^2 v \left[\frac{q_v(z) - q_v(z_{0E})}{\ln(z/z_0) \ln(z/z_{0E})} \right],
 \end{aligned} \tag{3}$$

300 where z_0 , z_{0H} , and z_{0E} are the roughness length scales for momentum, heat and moisture fluxes
 301 (m), z is the measurement height for wind, temperature, and humidity (typically 2 m), ρ_a is air
 302 density (kg m^{-3}), c_{pa} is the specific heat capacity of air ($\text{J kg}^{-1} \text{°C}^{-1}$), $L_{s/v}$ is the latent heat of
 303 sublimation or evaporation (J kg^{-1}), $k = 0.4$ is von Karman's constant, and K denotes the

turbulent eddy diffusivities ($\text{m}^2 \text{s}^{-1}$). Implicit in Eq. (3) is an assumption that the eddy diffusivities for momentum, sensible heat, and latent heat transport are equal. Eq. (3) also assumes neutral stability in the glacier boundary layer, although this can be adjusted to parameterize the effects of atmospheric stability. This tends to reduce the turbulent energy exchange due to the stable glacier boundary layer.

I adopt surface values for the near-surface layer, $T_0(z_{0H}) = T_s$ and $q_v(z_{0E}) = q_s$, assuming a saturated air layer at the glacier surface (e.g., Oerlemans, 2000; Munro, 2004). With this treatment, Eq. (3) is equivalent to the bulk transport equations for turbulent flux,

$$\begin{aligned} Q_H &= C_H v [T_a(z) - T_s] , \\ Q_E &= C_E v [q_v(z) - q_s] . \end{aligned} \tag{4}$$

where C_H and C_E are bulk transfer coefficients that absorb the constants and the roughness values in Eq. (3), as well as stability corrections.

The point energy balance model is calibrated and evaluated at the GAWS site based on ultrasonic depth gauge melt estimates in combination with snowpit-based snow density measurements. Local albedo measurements also assist with this, in indicating the date of transition from seasonal snow to exposed glacier ice. Surface roughness values are tuned to achieve closure in the energy balance (e.g., Braun and Hock, 2004), adopting $z_{0H} = z_{0E} = z_0/100$ (Hock and Holmgren, 2005). I work with Eq. (3) in this study, to permit direct consideration of roughness values, but this effectively reduces to the bulk transport equations, with stability corrections embedded in the roughness coefficients.

3.3 Distributed Model

Glacier-wide runoff estimates require distributed meteorological and energy balance fields (e.g., Arnold et al., 1995; Klok and Oerlemans, 2002), along with characterization of glacier surface albedo and roughness. Meteorological forcing across the glacier is based on 30-minute GAWS data for the period May 1 to September 30, which spans the melt season. Following the methods described in section 3.1, FFAWS data is used where GAWS data are unavailable. If FFAWS data are also missing for a particular field, average GAWS values for that day are used as a default, based on the available observations from 2002-2012. The glacier surface is represented using a digital elevation model (DEM) derived from 2005 Aster imagery, with a resolution of 1 arcsec, giving grid cells of 22.5 m × 35.8 m.

Distributed meteorological forcing requires a number of approximations regarding either homogeneity or spatial variation in meteorological and energy-balance fields. For incoming shortwave radiation, slope, aspect, and elevation are taken into account through the calculation of local potential direct solar radiation, $Q_{S\phi}$ (Oke, 1987),

$$Q_{S\phi} = I_0 \left(\frac{R_0}{R} \right)^2 \cos(\Theta) \varphi^{p/p_0 \cos(Z)}, \quad (5)$$

where I_0 is the solar constant, R and R_0 are the instantaneous and mean Earth-Sun distance, φ is the clear-sky atmospheric transmissivity, p is the air pressure, and p_0 is sea-level air pressure. Angle Z is the solar zenith (i.e. sun angle), which is a function of the time of day, day of year, and latitude, and Θ can be thought of as the effective local solar zenith angle, taking into account terrain slope and aspect (Oke, 1987). For a horizontal surface, $\Theta = Z$.

For each grid cell, total daily potential direct shortwave radiation is calculated through integration of Eq. (5) from sunrise to sunset. This is done at 10-minute intervals, including the

effects of local topographic shading based a regional DEM, i.e. examining whether a terrain obstacle is blocking the direct solar beam (e.g., Arnold et al., 1996; Hock and Holmgren, 2005). This spatial field $Q_{S\phi}(x,y)$ is pre-calculated for each grid cell for each day of the year, using a clear-sky transmissivity $\psi = 0.78$. This value is based on calibration of Eq. (5) at the two AWS sites for clear-sky summer days, using $\Theta = Z$ (the radiometer is mounted horizontally). Diffuse shortwave radiation, Q_d , also needs to be estimated, as there is a diffuse component to the measured radiation, Q_S^\downarrow . I assume that mean daily Q_d equals 20% of the potential direct solar radiation, after Arnold et al. (1996). Assuming that the mean daily diffuse fraction and clear-sky transmissivity are constant through the summer, observed daily solar radiation on clear-sky days can then be compared with theoretical values of incoming radiation, $Q_{S\phi} + Q_d$, to determine the effective value of ψ .

Temporal variations in incoming shortwave radiation due to variable cloud cover or aerosol depth are characterized by a mean daily sky clearness index, c , calculated from the ratio of measured to potential incoming solar radiation at the GAWS: $c = Q_S^\downarrow / (Q_{S\phi} + Q_d)$. For clear-sky conditions, $c = 1$. This is assumed to be uniform over the glacier: essentially an assumption that cloud conditions are the same at all locations. Daily incoming solar radiation at point (x,y) can then be estimated from $Q_S^\downarrow(x,y) = c[Q_{S\phi}(x,y) + Q_d(x,y)]$.

Incoming longwave radiation is also taken to be uniform over the glacier, using the measured GAWS value. Where this is unavailable, an empirical relation developed at Haig Glacier is used,

$$Q_L^\downarrow = \varepsilon_a \sigma T_a^4 = (a_\varepsilon + b_\varepsilon e_v / e_s + c_\varepsilon e_v) \sigma T_a^4, \quad (6)$$

where $\sigma = 5.67 \times 10^{-8} \text{ W m}^{-2} \text{ K}^{-4}$ is Stefan-Boltzmann's constant, ε_a is the atmospheric emissivity, and T_a is the 2-m absolute air temperature. Empirical formulations for Q_L^\downarrow at Haig Glacier have been examined as a function of numerous meteorological variables (manuscript under review), and vapour pressure and relative humidity provide the best predictive skill for Q_L^\downarrow , for the relation $\varepsilon_a = a_\varepsilon + b_\varepsilon e_v/e_s + c_\varepsilon e_v$. Here, relative humidity is expressed as the ratio of vapour pressure over saturation vapour pressure, $e_v/e_s \in [0,1]$. Parameters a_ε , b_ε and c_ε are locally calibrated and are held constant (Table 2). Eq. (6) gives an improved representation of 30-minute and daily mean values of Q_L^\downarrow at Haig Glacier relative to other empirical formulations that we have tested for all-sky conditions (e.g., Lhomme et al., 2007; Sedlar and Hock, 2010).

Outgoing shortwave and longwave radiation are locally calculated, as a function of albedo, α_s , and surface temperature, T_s : $Q_s^\uparrow = \alpha_s Q_s^\downarrow$ and $Q_L^\uparrow = \varepsilon_s \sigma T_s^4$. Parameter ε_s is the thermal emissivity of the surface (~ 0.98 for snow and ice and ~ 1 for water) and T_s is the absolute temperature. On a melting glacier with a wet surface, $\varepsilon_s \rightarrow 1$, $T_s = 273.15 \text{ K}$ and $Q_L^\uparrow \approx 316 \text{ W m}^{-2}$. Albedo and surface temperature are modeled in each grid cell as a function of the local snowpack evolution through the summer (see below for more on the albedo model).

Turbulent fluxes are estimated at each site from Eq. (3). Wind speed is assumed to be spatially uniform while temperature and specific humidity are assumed to vary linearly with elevation on the glacier, with lapse rates β_T and β_q . The temperature lapse rate is set to -5°C km^{-1} , based on summer data from the elevation-transect of Veriteq temperature sensors. Note that this is a different approach from the temperature transfer function between the FFAWS and GAWS sites, as only the glacier surface environment is being considered, with similar energy balance processes governing near-surface temperature.

In contrast, specific humidity variations in the atmosphere are driven by larger-scale air mass, rainout, and thermodynamic constraints, which are affected by elevation but not necessarily the surface environment. Estimates of β_q are based on the mean daily gradient between the FFAWS and GAWS sites. Given local temperature and humidity, air pressure and density are calculated as a function of elevation from the hydrostatic equation and ideal gas law, using FFAWS pressure data as described above. This gives the full energy balance that is needed to estimate 30-minute melt totals (or if $Q_N < 0$, refreezing or temperature changes) at all points on the glacier.

Local albedo modeling is necessary to estimate absorbed solar radiation, the largest term in the surface energy balance for mid-latitude glaciers (e.g., Greuell and Smeets, 2001). This in turn requires an estimate of the initial snowpack, based on May snowpack measurements from each year. As the snowpack melts, albedo declines as a result of liquid water content, increasing concentration of impurities, and grain growth (Cuffey and Patterson, 2010). Brock et al. (2000) showed that these effects can be empirically approximated as a function of cumulative melt or maximum daily temperatures. We have adapted this suggestion and represent the snow-albedo decline through the summer melt season as a function of cumulative positive degree days, $\sum PDD$ (Hirose and Marshall, 2013),

$$\alpha_s(t) = \max [\alpha_0 - b \sum PDD(t), \alpha_{\min}], \quad (7)$$

for fresh-snow albedo α_0 , minimum snow albedo α_{\min} , and coefficient b . Nonlinear (e.g., exponential) decay of albedo can also be parameterized in lieu of Eq. (7). Once seasonal snow is depleted, surface albedo is set to observed values for firn or glacial ice at Haig Glacier, $\alpha_f = 0.4$

and $\alpha_i = 0.25$. The firn zone on the glacier is specified based on its observed extent, at elevations above 2710 m, and is spatially fixed.

Fresh snowfall in summer is assigned an initial albedo of α_0 and declines, following Eq. (7), until the underlying surface is exposed again, with an albedo equal to its pre-freshened value. Summer precipitation events are modeled as random events, with the number of events from May through September, N_P , treated as a free variable (Hirose and Marshall, 2013). The amount of daily precipitation within these events is modeled with a uniform random distribution, varying from 1 to 10 mm. Local temperatures dictate whether this falls as rain or snow at the glacier grid cells, with snow assumed to accumulate when $T < 1^\circ\text{C}$.

Parameter values in the distributed meteorological and energy balance models are summarized in Table 2. The energy balance equations are solved to compute 30-minute melt and meltwater that does not refreeze is assumed to run off within the day. Half-hour melt totals can then be aggregated for each day and for all grid cells to give modeled daily runoff.

4. Results

4.1 Snowpack Observations

Winter mass balance on the glacier averaged 1360 mm water equivalent (w.e.) from 2002-2013, with a standard deviation of 230 mm w.e. (Table 3). The spatial pattern of winter snow loading recurs from year to year, in association with snow redistribution from down-glacier winds interacting with the glacier topography (e.g., snow scouring on convexities; snow deposition on the lee side of the concavity at the toe of the glacier). Lateral snow-probing transects reveal some systematic cross-glacier variation in the winter snowpack, but snow depths on the lateral transects are typically within 10% of the centreline value. More uncertain are steep, high-


elevation sections of Haig Glacier along the north-facing valley wall (Figure 1). These sites cannot be sampled, so all elevations above French Pass (2750 m) are assumed to have constant winter SWE, based on the value at French Pass.

In most years the snowpack is still dry and is below 0°C during the May snow survey, with refrozen ice layers present from episodic winter or spring thaws. By late May, the snowpack has ripened to the melting point, there is liquid water in the snowpack pore space, and runoff may have commenced at the lowest elevations.

The winter snowpack as measured is an approximation of the true winter accumulation on the glacier, sometimes missing late-winter snow and sometimes missing some early-summer runoff. Assuming an uncertainty of 10% associated with this, combined with the independent 10% uncertainty arising from spatial variability, the overall uncertainty in winter mass balance estimates can be assessed at $\pm 14\%$. The melt model is initiated on May 1 for all years. While this is not in accord with the timing of the winter snow surveys, there is generally little melting and runoff through May (see below); model results are not sensitive to the choice of e.g., May 1 vs. May 15. The May 1 initiation allows the snowpack ripening process to be simulated and allows the possibility of early season melt/runoff in anomalously warm springs.

4.2 Meteorological Observations

Table 4 presents mean monthly, summer, and annual meteorological conditions measured at the GAWS. Monthly values are based on the mean of all available days with data for each month from 2002-2012. Figure 2 depicts the annual cycle of temperature, humidity and wind at the two AWS sites, as well as average daily radiation fluxes at the glacier AWS. Values in the figure are mean daily values for the multi-year dataset.

On average, the GAWS site is cooler, drier, and windier than the glacier forefield. Mean annual wind speeds at the glacier and forefield AWS sites are 3.2  and 3.0 m/s, respectively, although the FFAWS site experiences stronger summer winds. Winter (DJF) winds averaging 4.0 m/s. This is calm for a glacial environment, although there are frequent wind storms at the site; peak annual 10-second wind gusts average 23.7 m/s on the glacier (85 km/h) and 26.3 m/s (95 km/h) at the forefield site. Katabatic winds are not well-developed or persistent at Haig Glacier. The low wind speeds and variable wind direction (not presented) indicate that the glacier is primarily subject to topographically-funnelled synoptic-scale winds.

Mean annual and mean summer temperatures derived from the GAWS data are -4.2°C and $+5.0^{\circ}\text{C}$, respectively. This compares with values of -1.3°C and $+8.1^{\circ}\text{C}$ at the FFAWS. The pattern of monthly temperature differences between the forefield and glacier sites is of interest, as it is commonly necessary to estimate glacier conditions from an off-glacier site in glaciological studies. Mean daily temperature differences between the two sites were calculated based on all available days with temperature data from both AWS sites ($N = 2084$). This data forms the basis of the temperature offset used to reconstruct temperatures on the glacier when data are missing at the GAWS.

Monthly temperature differences are plotted in Fig. 3b, expressed as both monthly offsets and as lapse rates. Temperature gradients are stronger in the summer months at Haig Glacier, with a mean of $-9.3^{\circ}\text{C km}^{-1}$ from July through September. This compares with a mean annual value of $-7.1^{\circ}\text{C km}^{-1}$. This is not a true lapse rate, i.e. a measure of the rate of cooling in the free atmosphere. Rather, temperature offsets are governed by the local surface energy balance and the resultant near-surface air temperatures at each site. The larger difference in summer temperatures

can be attributed to the strong warming of the forefield site once it is free of seasonal snow (or equivalently, a glacier cooling effect).

4.3 Surface Energy Balance

Figure 4 plots the shortwave radiation budget and albedo evolution at the two AWS sites, illustrating this summer divergence. Net shortwave radiation is similar at the two sites through the winter until about the second week of May, after which time the GAWS maintains a higher albedo until mid-October, when the next winter sets in. Bare rock is typically exposed at the FFAWS site for about a three-month period from mid-June until mid-September, with intermittent snow cover in September and early October. In wet years, snow persists into early July, with the FFAWS snow-free by July 10 in all years of the study. These dates provide a sense of the high-elevation seasonal snow cover on non-glacierized sites in the region. Meltwater runoff from the Canadian Rocky Mountains is primarily glacier-derived (a mix of snow and ice) from mid-July through September.

The albedo data also provide good constraint on the summer albedo evolution and the bare-ice albedo at this site. The mean annual GAWS albedo value is 0.75, with a summer value of 0.55 and a minimum in August, 0.41. The GAWS was established near the median glacier elevation, in the vicinity of the equilibrium line altitude for equilibrium mass balance: ELA_0 , where net mass balance $b_a = 0$. The glacier has not experienced a positive mass balance during the period of study, with the snowline always advancing above the GAWS site in late summer. The transition to snow-free conditions at the GAWS occurred from July 23 to August 20 over the period of study, with a median date of August 5. Bare ice is exposed beyond this date until the start of the next accumulation season in September or October. The mean measured GAWS ice

albedo over the full record is 0.25, with a standard deviation of 0.04. This value is applied for exposed glacier ice in the glacier-wide melt modeling.

Table 5 summarizes the average monthly surface energy balance fluxes at the GAWS. Peak temperatures and positive degree days are in July, but maximum net energy, Q_N , and meltwater production occur in August due to the lower surface albedo. Net energy over the summer (JJA) averages 85 W m^{-2} , peaking in August at 109 W m^{-2} . Net radiation, Q^* , averages 63 W m^{-2} and makes up 74% of the available melt energy. Turbulent fluxes account for the remaining 26%, with 25 W m^{-2} from sensible heat transfer to the glacier and a small, negative offset associated with the latent heat exchange. Sensible heat flux plays a stronger role at the GAWS in the month of July (34% of available melt energy). Monthly mean values of Q^* , Q_H , and net energy, Q_N , are plotted in Figure 5. To first order, $Q_N \approx Q^* + Q_H$ through the summer melt season, with monthly mean conductive and evaporative heat fluxes less than 10 W m^{-2} . Average annual melting at the GAWS is $2234 \pm 375 \text{ mm w.e.}$, of which 2034 mm (91%) is derived in the months of June through August. Summer melt ranged from 1610-2830 mm from 2002-2012. Mean daily and monthly melt totals are plotted in Fig. 5b.

4.4 Distributed Energy and Mass Balance

The distributed energy balance model is run from May through September of each year based on May snowpack initializations and 30-minute AWS data from 2002-2013. This provides estimates of surface mass balance and glacier runoff for each summer (Table 6). Glacier-wide winter snow accumulation, B_w , averaged $1360 \pm 230 \text{ mm w.e.}$ over this period, with summer snowfall contributing an additional $50 \pm 14 \text{ mm w.e.}$ This is countered by an average annual melt of $2350 \pm 590 \text{ mm w.e.}$, giving a specific surface mass balance of $B_a = -960 \pm 580 \text{ mm w.e.}$ Specific

mass balance ranged from -2300 to -340 mm w.e. from 2002-2013; the glacier has not experienced a positive annual mass balance during the period of study. Cumulative mass loss from 2002-2013 equates to an areally-averaged glacier thinning of 11.4 m w.e. (12.5 m of ice).

An example of the modeled summer melt and net mass balance as a function of elevation for all glacier grid cells is plotted in Figure 6, for the summer of 2012. This year is representative of mean 2002-2013 conditions at the site, with $B_a = -880$ mm w.e. Summer melt totals at low elevations on the glacier were about 3600 mm w.e., decreasing to about 1000 mm w.e. on the upper glacier (Fig. 6a). Some grid cells above 2650 m altitude experienced net accumulation this summer ($b_a > 0$ in Fig. 6b), but there was no simply-defined equilibrium line altitude (end of summer snowline elevation). This is due to differential melting as a function of topographic shading and other spatial variations in the snow accumulation and energy balance processes. Mass losses in the lower ablation zone exceeded 2000 mm w.e. Melt and mass balance gradients are non-linear with elevation and are steepest on the upper glacier.

Model results are in accord with observations of extensive mass loss at the site over the study period. The snowline retreated above the glacier by end of summer (i.e. with no seasonal snow remaining in the accumulation area) in 2003, 2006, 2009 and 2011. Surface mass balance was measured on the glacier from 2002-2005: $B_a = -330, -1530, -700$ and -650 mm w.e., respectively. Observed values are in reasonable accord with the model estimates, with an average error of $+20$ mm w.e. and an average absolute error of 160 mm w.e. The model underestimates the net balance for two of the years and overestimates it the other two.

Figure 7a plots measured vs. modeled melt for all available periods with direct data (snow pits or ablation stakes) at the GAWS. Data shown are for different time periods from 2002-2012,

ranging from two weeks to three months. The fit to the data is good ($R^2 = 0.89$, slope of 1.0), with an RMS error of 170 mm w.e. The multi-week integration period averages out day-to-day differences between observations and the model. A plot of measured vs. modeled daily net energy balance shows more scatter (Fig. 7b), with an RMS error in daily net energy of 38 W m^{-2} . Scatter arises mostly due to discrepancies in actual vs. modeled albedo. Although there are direct albedo measurements that could be used in the model at the GAWS site, these are not available glacier-wide. For consistency, the albedo is therefore modeled via Eq. (5) at the GAWS. Where the simulated snow-to-ice transition occurs earlier or later than in reality, this gives systematic over- or under-estimates of the net energy available for melt.

There are also departures associated with actual vs. modeled summer snow events. On average, the stochastic precipitation model predicts 9.2 ± 2.1 snow days per summer (out of 25 summer precipitation events). This is in good accord with the number of summer-snow events inferred from GAWS albedo measurements. The correct timing of summer snow events is not captured in the stochastic summer precipitation model that is used, so the effects of summer snow on the snow depth and albedo are not accurately captured with respect to timing. For monthly or seasonal melt totals, this is unlikely to be a concern, but albedo-melt feedbacks could cause the stochastic model to diverge from reality. For this reason 30 realizations of the distributed model are run for each summer, with identical meteorological forcing, initial snowpack, and model parameters. Values reported in Table 6 are the averages from this ensemble of runs. The standard deviation of the net balance associated with the stochastic summer-snow model is 87 mm w.e. Of this stochastic variability, about 20% is due to the direct mass balance impact of summer snowfall and 80% arises from the melt reduction due to increased albedo.

Glacier summer (JJA) temperature ranged from 4.1 to 6.5°C over the 12 years, with a mean and standard deviation of $5.0 \pm 0.8^\circ\text{C}$. Where \pm values are included in the results and in the tables, it refers to ± 1 standard deviation, which is reported to give a sense of the year-to-year variability. Mean summer albedo from 2002-2013 was 0.57 ± 0.04 , ranging from 0.48 to 0.64. The most extensive melting on record occurred in the summer of 2006, which had the highest temperature, the lowest albedo, and the greatest net radiation totals, an example of the positive feedbacks associated with extensive melting. On average, glacier grid cells experienced melting on 130 out of 153 days from May to September in 2006, compared with an average of 116 ± 8 melt days. Summer 2010 offers a contrast, with the lowest number of melt days (103), the lowest temperature, and the highest albedo. This gave limited mass loss in 2010, despite an unusually thin spring snowpack. Summer temperatures and melt extent are generally more influential on net mass balance than winter snowpack at this site. Winter mass balance is only weakly correlated with net balance ($r = 0.16$), whereas summer and net balance are highly correlated ($r = -0.93$). Net balance is also significantly correlated with summer temperature ($r = -0.56$), *PDD* ($r = -0.69$), albedo ($r = 0.86$), and net radiation ($r = -0.89$).

4.5 Glacier Runoff

With the assumption that no surface melt is stored in the glacier, modeled specific runoff from the glacier from 2002-2013 was 2350 ± 590 mm w.e., ranging from 1490 to 3690 mm w.e. These values exceed the mean and range from the GAWS site because melt rates increase non-linearly at lower elevations. Table 7 gives the mean monthly and summer runoff from all years. On average, meltwater derived from glacier ice and firn constitutes $42 \pm 14\%$ of total summer runoff. During the warm summer of 2006, glacier- and firn-derived meltwater made up 62% of

total runoff. In most years, more than half of the runoff originates from seasonal snowmelt, the bulk of which is generated in the months of May through July. Runoff provenance shifts in August and September, with ice and firn melt representing 62 and 92% of runoff in these months (Table 7).

Figure 8 plots the average daily melt and the cumulative summer melt derived from seasonal snow and from the ice/firn reservoir. The average snowpack depletion curve is also plotted in Figure 8b. The first appreciable glacier melt begins in mid-July and runoff typically switches from snow- to ice-dominated around the second week of August. Snowmelt runoff continues through the month of August, declining steadily as the snowline advances up the glacier.

Direct stream runoff measurements from the glacier illustrate the nature of the melt-discharge relationship on Haig Glacier. Figure 9 plots measured discharge from July 24 to September 22, 2013, a period when the glacier drainage system was well-established. Insolation-driven daily melt cycles produce a strong diurnal discharge cycle, typical of alpine glacier outlet streams (Fountain and Tangborn, 1985). Periods of high overnight flows reflect either rain events or warm nights, when melting did not shut down on the glacier (e.g., the third week of August). The end of summer is evident in the discharge record, with low flows commencing after Sept. 20. New snow cover was beginning to accumulate on the glacier at this time, and the baseflow recorded through this period probably reflects residual summer meltwater that is still being evacuated through the subglacial drainage system.

The diurnal cycle and lags between melt and stream discharge are shown more clearly in Figure 10, which plots modeled glacier melt and the observed stream discharge over an 8-day period in late summer. Peak runoff lags maximum snow/ice melt by an average of 3.5 hours

606 over the summer, based on the time lag of peak correlation between the two time series. The
607 runoff curve is more diffuse, with a broader daily peak. Meltwater generation shuts down
608 rapidly on most nights in late summer, while the discharge hydrograph has a broader recession
609 limb. This is a consequence of different meltwater pathways and travel distances through the
610 glacier drainage system.

611 The period of measurements of glacier runoff is limited and is biased to the late summer, when
612 the glacier surface is mostly exposed ice, so it is difficult to use this data to test or constrain the
613 melt model. Lags in runoff relative to meltwater generation are likely to evolve through the
614 summer melt season, with the value of 3.5 hours noted above specific to the second half of the
615 ablation season, when meltwater drainage pathways are well-developed. Nevertheless, some
616 comparison of measured stream discharge vs. modeled meltwater runoff is possible. For the
617 periods where stream data is available, the maximum lagged correlation between daily totals of
618 discharge and meltwater runoff is $r = 0.65$, for a time lag of two days.

619 Total modeled meltwater over the 60-day record in Figure 9 is equal to $4.73 \times 10^6 \text{ m}^3$, which is
620 88% of the measured discharge over this period, $5.38 \times 10^6 \text{ m}^3$. The runoff totals are
621 equivalent, given the uncertainties in both the melt model and the stream ratings curve.

622 Rainfall contributions to streamflow are also neglected here, and may explain much of the
623 difference. We do not have rainfall data from the site in summer 2013. Similar relations were
624 found in summer 2014 (data not shown), with modeled runoff equal to 89% of the measured
625 discharge and daily stream discharge lagging modeled daily runoff by two days. This additional
626 runoff data and a more detailed examination of the hydrological drainage characteristics at the
627 site are the subject of ongoing study, to be presented elsewhere.

5. DISCUSSION

5.1 Meteorological and Hydrological Conditions

Meteorological and mass balance data collected at Haig Glacier provide insights into the hydrometeorological regime of glaciers in the Canadian Rocky Mountains. From 2002-2013, the mean annual and summer (JJA) temperatures at 2670 m altitude at the Haig Glacier AWS were -4.2°C and 5.0°C . Mean winter (October to May) snow accumulation at the AWS site was 1230 mm w.e. over this period. Glacier-wide average May snowpack was 1360 mm w.e., reaching 1700 mm w.e. in the upper accumulation area on the glacier.

The corresponding values at the forefield AWS, at 2340 m altitude, are -1.3°C , 8.1°C and 770 mm w.e. These measurements illustrate the steep temperature and precipitation lapse rates with elevation between the forefield and glacier environments. Expressed as a lapse rate, the annual and summer temperature gradients between the FFAWS and GAWS sites are $-8.8^{\circ}\text{C km}^{-1}$ and $-9.4^{\circ}\text{C km}^{-1}$, while winter snow accumulation on the glacier is 180% of that at the FFAWS. The strong temperature gradient is a result of the ‘glacier cooling’ effect; surface temperatures cannot rise above 0°C during the summer melt season, fostering a cold air mass over the glacier. High snow accumulation on the glacier is partly due to its higher elevation and its position on the continental divide, where it intercepts moist, westerly air masses, and partly because the glacier surface is effective at retaining early- and late-season snow.

The differences in climatology over a distance of 2.1 km between the AWS sites illustrate some of the difficulty in modeling glacier energy and mass balance without *in situ* data. It can be even more difficult to estimate glacier conditions based on distal (e.g. valley bottom) data, as is often necessary. Longterm meteorological data from Banff, Alberta (*Environment Canada*, 2014) is

probably the best available data to assess the historical glacier evolution in the Canadian Rocky Mountains, but the site is at an elevation of 1397 m and in a snow shadow relative to locations along the continental divide (Shea and Marshall, 2007). October to May precipitation in Banff averaged 225 mm w.e. from 2002-2013, 17% of that on Haig Glacier. Conditions become drier as one moves east from the continental divide, as discussed above with respect to Calgary, Alberta. It is difficult to apply a realistic precipitation-elevation gradient in mountain regions, as is often necessary in glacier mass balance modeling (e.g., Nolin et al., 2010; Jeelani et al., 2012). This challenge may be exacerbated when one is not on the windward side of the mountain range, within the classical orographic precipitation belt.

Temperatures are also difficult to map. Relative to Banff, the Haig Glacier AWS site is 6.9°C cooler over the year and 8.3°C cooler in the summer months, effective lapse rates of $-5.4^{\circ}\text{C km}^{-1}$ and $-6.5^{\circ}\text{C km}^{-1}$, respectively. These are much different vertical temperature gradients than one would adopt based on the FFAWS vs. GAWS data, reflecting the different meteorological and surface environments. High elevations in the Canadian Rocky Mountains are subject to strong westerly (mild, Pacific) influences, which commonly situate the glaciers above the inversion layer when cold air masses are present in the Canadian prairies.

The choice of temperature lapse rates is critical in glacier melt modeling, but the most appropriate values to use are generally unknown. Daily or monthly temperature offsets ΔT are recommended to translate off-glacier temperature records to a reference site on the glacier. A near-surface temperature lapse rate specific to the glacier boundary layer can then be applied to extrapolate temperatures to different elevations on the glacier. Temperature gradients in the

glacier boundary layer are commonly weaker than free-air lapse rates (e.g., Braun and Hock, 2004; Marshall et al., 2007).

5.2 Surface Energy and Mass Balance

Temperature and precipitation conditions discussed above, along with wind, radiation, and humidity data from the site, offer insights into the climatology of glacierized regions in the Canadian Rocky Mountains, although Haig Glacier is in disequilibrium with these conditions. The relation between net mass balance and summer temperature is $\partial B_a / \partial T = -420 \text{ mm w.e. } ^\circ\text{C}^{-1}$. For the mean mass balance of -960 mm w.e. during the study period, this indicates that – all else equal – conditions 2.3°C cooler would be needed to give a state of balance, $B_a = 0$. Alternatively, a 70% increase in snow accumulation would be required. The glacier likely developed under a climate state that was both cooler and wetter, with summer temperatures below 3°C .

As has been demonstrated at other mid-latitude glacier sites (e.g., Greuell and Smeets, 2001; Klok and Oerlemans, 2002), net radiation provides about 75% of the available melt energy at Haig Glacier over the summer melt season, with sensible heat flux contributing the rest. Latent heat flux and net longwave radiation act as energy loss terms in the summer. Modeled glacier-wide values are similar to those at the GAWS site, with about 10% less incoming solar radiation and similar annual melt totals. The differences are likely because much of the glacier experiences more topographic shading than the GAWS site, but lies at lower (i.e. warmer) altitudes.

The annual time series is limited ($N = 12$), but for the available data, annual net mass balance at Haig Glacier is negatively correlated with summer temperature, PDD , net shortwave radiation, net radiation, and sensible heat flux (linear correlation coefficients between $r = -0.61$ and $r = -0.89$), and there is a strong positive correlation with average summer albedo ($r = 0.90$). There is

no significant correlation between winter and net mass balance; summer weather conditions were the dominant control on interannual mass balance variability over this period.

The relation between net mass balance and mean summer radiation budget is stronger than the B_a - T relation, and is mostly associated with variations in absorbed solar radiation. Observations indicate a mass balance sensitivity $\partial B_a / \partial Q_{s_{net}} = -42 \text{ mm w.e. (W m}^{-2}\text{)}^{-1}$. This encompasses variations in winter snowpack and summer snowfall (through their influence on surface albedo), cloud cover (i.e. incoming solar radiation), and the strength of the summer melt season, with its associated albedo feedbacks. Albedo is the dominant influence, with a sensitivity $\partial B_a / \partial \alpha_s = +145 \text{ mm w.e. \%}^{-1}$. For instance, a mean summer albedo change of ± 0.1 is associated with $\Delta B_a = \pm 1450 \text{ mm w.e.}$ Because of this high sensitivity, it is difficult to separate the role of temperature and absorbed solar radiation in the surface energy budget; mean summer temperature and albedo are strongly correlated in the observational record ($r = -0.75$). In general, temperature and solar radiation collaborate in driving years of high or low mass balance, mediated through albedo feedbacks.

The distributed energy balance model predicts melt estimates in good accord with available observations, although these are limited to point measurements at the GAWS site and four years of surface mass balance data. Direct observations of the annual snowline retreat (end of summer ELA and accumulation-area ratio, AAR) are consistent with the modeled end-of-summer snowline and the finding that the glacier has experienced a consistently negative annual mass balance over the period of study.

Estimates of glacier mass loss and thinning over the study period also reflect net mass balance measurements from Peyto Glacier, Alberta, which are available from 1966-2012 (*Demuth et al.*,

2008; WGMS, 2014). Peyto Glacier is situated 140 km northwest of Haig Glacier (Fig. 1) and it is an outlet of the Wapta Icefield, flowing eastward from the continental divide in the Canadian Rocky Mountains. Surface mass balance data from Peyto Glacier indicate a cumulative thinning of about 29 m (ice equivalent) from 1966-2012 and 9.9 m for the period 2002-2012. This compares with 10.6 m of thinning at Haig Glacier for the period of overlap of the observations, from 2002-2012. Net specific mass balance averaged $-820 \text{ mm w.e. yr}^{-1}$ at Peyto from 2002-2012 and $-880 \text{ mm w.e. yr}^{-1}$ at Haig. Net mass balance was negative at both sites for all years in this period, with the annual net mass balance values positively correlated ($r = 0.64$).

5.3 Glacier Runoff in the Canadian Rocky Mountains

Snowpack depth and specific runoff at glaciers in the Canadian Rockies are exceptional within the context of the Bow River basin, which spans a steep climatic gradient from the semi-arid southern Canadian prairies to the Rocky Mountains. Average naturalized flows in the Bow River basin are estimated at $3.95 \times 10^9 \text{ m}^3$ (BRBC, 2005). Over the basin area of $25,120 \text{ km}^2$, this gives a specific runoff of 160 mm. Upstream of Calgary, the Bow River drains an area of 7895 km^2 , with naturalized annual flows of $2.53 \times 10^9 \text{ m}^3$ from 2000-2009: a specific runoff of 320 mm. This is twice the specific runoff of the entire basin, reflecting the proximity of Calgary to the high-elevation source regions where there is greater precipitation and less evapotranspiration. Nevertheless, 320 mm compares with 2350 mm of glacier-derived specific runoff from 2002-2013. As landscape elements, glaciers contribute disproportionately to streamflow, by a ratio of more than 7:1 upstream of Calgary and 15:1 over the Bow basin. Their overall importance to basin-scale water resources is limited by the extent of glacierized area in the basin. Based on a satellite-derived glacier inventory (Bolch et al., 2009), glaciers made up 60 km^2 of the Bow

River basin in 2005. This represents 0.24% of the basin and 0.76% of the area upstream of Calgary. Assuming that the mean specific runoff measured at Haig Glacier is representative of all the glaciers in the Bow basin, average glacier discharge (combined snow and ice melt) from 2002-2013 can be estimated at $0.14 \times 10^9 \text{ m}^3 \text{ yr}^{-1}$. This is 3.6% of annual flow in the Bow basin and 5.6% of annual flow in Calgary. These values include contributions from the seasonal snowpack, which represented about 60% of glacier runoff over the study period. Contributions from glacier storage – glacier ice and firn – averaged $0.06 \times 10^9 \text{ m}^3 \text{ yr}^{-1}$ from 2002-2013, 1.5% and 2.3% of annual flow in the Bow basin and in Calgary, respectively.

Over the months of July to September, when glacier ice and firn dominate the runoff, naturalized Bow River flows in Calgary were $1.01 \times 10^9 \text{ m}^3$ from 2000-2009 (Marshall et al., 2011). On average, runoff from ice and firn melt constitutes 5.6% of the flow over these months, and more than 14% during warm, dry summers such as 2006, when $0.14 \times 10^9 \text{ m}^3$ of water was released from glacier storage. This is significant in the context of late-summer water demands for municipal and agricultural allocations, which tend to be acute during warm, dry summers.

These numbers are based on the assumption that glacier runoff enters the river system within the months of July to September, without significant losses to evaporation or delays due to groundwater infiltration. Glacial streams are channelized, draining down steep gradients in the mountains, so initial losses and delays in transit are likely to be minimal, but some of the glacier meltwater will enter the groundwater drainage system and will also be delayed through storage in downstream lakes and reservoirs. Summer runoff contributions to the Bow River presented here should therefore be taken as maximum estimates.

758 These simulations also neglect changes in runoff associated with glacier geometric changes over
759 the study period. The DEM used to drive the model is from 2005, so is reasonably representative
760 of conditions over the study period (2002-2013), but the glacier retreated by about 40 m over this
761 time, with an associated loss in area of about 2%. A sensitivity study carried out with the melt
762 model indicates that a 2% decrease in glacier extent, introduced at the terminus, reduces summer
763 runoff by 2.6%. For a glacier area loss of 5%, modeled runoff declines by 6.6%. The relation is
764 nonlinear because melt rates at the glacier terminus exceeds average values over the glacier.
765 There is also a small effect from glacier thinning over the study period, which acts in the other
766 direction (i.e., increased discharge as the glacier thins), but this is weaker than the effect of
767 glacier area changes. Overall, glacier retreat from 2002-2013 gives summer runoff estimates in
768 Table 7 that are a bit too low for the early years of the study and slightly overestimated post-
769 2005, but the errors associated with neglecting glacier geometric changes are assessed to be less
770 than 2%. Longer-term glacier-hydrological studies would need to accommodate glacier
771 geometric adjustments, however.

772 Results provide observationally-based support for previous estimates of glacier contributions to
773 the Bow River based on basin-scale modeling (Comeau et al., 2009; Marshall et al., 2011; Bash
774 and Marshall, 2014). Prior modeling studies use relatively simple treatments of the glacier
775 geometry and surface energy balance/melt processes, and don't clearly capture the separate
776 contributions of snow and ice melt. Similarly, runoff data from hydrometric gauging stations
777 include combined contributions from both seasonal snow and glacier ice/firn. Observations and
778 modeling presented here provide insight into the provenance and timing of runoff. The results
779 indicate a large range of interannual variability in runoff derived from the ice/firn reservoir.

780 From 2002-2013, Haig Glacier specific runoff from ice/firn melt ranged from 420 to 2290 mm,
781 averaging 980 ± 560 mm. This constituted 19 to 62% of the total runoff from the glacier.

782 It is important to separate these components because the seasonal snowpack is intrinsically
783 renewable from year to year, while runoff derived from the long-term glacier storage reservoir is
784 declining as glaciers retreat (Moore et al., 2009). As in most mid-latitude mountain regions, this
785 reservoir dates to the Little Ice Age in the Canadian Rocky Mountains (17th to 19th century), and
786 is being steadily depleted in recent decades (e.g., Demuth et al., 2008; Moore et al., 2009). This
787 will compromise the ability of glaciers to buffer streamflow in warm, dry summers, as they have
788 historically done.

789 Glaciers remain third behind seasonal snowpack and spring/summer rainfall in overall
790 contributions to streamflow in the Bow Basin. Moreover, much of the flow in the Bow River and
791 in other critical rivers that issue from the Rocky Mountains is filtered through the groundwater
792 drainage system (Grasby et al., 1999), delaying downstream discharge of seasonal snow melt and
793 spring rains. This is responsible for most of the river discharge at low-elevation sites in the
794 Canadian prairies in late summer and fall, with the glaciers serving to top this up. The largest
795 concern with respect to future water supply is the spectre of declining mountain snowpack in
796 western North America (Mote et al., 2005; Barnett et al., 2005). It is likely that this is also
797 contributing to the widespread glacier decline, with positive feedbacks. Glaciers serve as highly
798 effective ‘snow traps’, accumulating snow in the early autumn through to early summer; the loss
799 of glaciers in the Rocky Mountains will contribute to declines in the spring snowpack at high
800 elevations, and associated runoff from seasonal snow melt.

The methodological approach developed here – a fully distributed energy balance model forced by 30-minute data – is probably excessive for estimation of monthly and annual runoff from the glacier, which is the main objective of this contribution. Daily mean meteorological variables and a simpler methodology, like temperature-index melt modeling, might give similar values for the monthly melt and runoff. Followup investigations are recommended to explore and quantitatively assess the level of sophistication and resolution that is warranted if one is only interested in monthly runoff or seasonal glacier mass balance.

6. CONCLUSIONS

Meteorological and surface energy balance data collected at Haig Glacier provides the first available decade-long measurements of year-round conditions from a glacier in the Canadian Rocky Mountains. These data give new insights into alpine meteorological and hydrological conditions and controls of glacier mass balance in the region. The glacier, which flows eastward from the North American continental divide, experiences relatively wet, mild conditions, with a climatology that has more in common with neighbouring British Columbia than the eastern slopes of the Canadian Rocky Mountains. Pacific moisture nourishes the glacier, while summer temperatures are typical of continental climate conditions, with a mean JJA temperature of 5°C and maximum daily temperatures over 15°C.

A distributed energy balance and melt model developed for Haig Glacier effectively captures interannual mass balance variations. Modeled mass balances are in good accord with data from Peyto Glacier, Alberta, and are likely representative of regional conditions. The energy balance model reveals the importance and inseparability of absorbed shortwave radiation, albedo and

822 temperature in determining summer melt extent. The summer melt season is more important than
823 winter snow accumulation for interannual mass balance variability at Haig Glacier.

824 Haig Glacier is well out of equilibrium with the climate conditions over the study period, 2002-
825 2013, with a succession of years of negative mass balance driving a cumulative glacier-wide
826 thinning of about 12.5 m over this period. A summer cooling of about 2.3°C, a 70% increase in
827 snowfall, or a combination of the two is needed to bring Haig Glacier into a state of balance.

828 This period of negative glacier mass balance is associated with high rates of specific discharge
829 from the glaciers, 2350 mm w.e., with this runoff generated in the May through September melt
830 season and concentrated in the months of July and August. This is an order of magnitude greater
831 than average recharge rates for the Bow River basin, and is likely to be typical of the glacier-fed
832 river basins that flow eastward from the Rocky Mountains into the Canadian prairies. However,
833 the overall contribution of glacier runoff to these rivers is limited by the relatively small area
834 with glacier cover, e.g., 0.23% in the case of the Bow River.

835 The model allows separation of glacier runoff derived from seasonal snow vs. the firn/ice storage
836 reservoir. Melting of the seasonal snowpack accounted for $58 \pm 14\%$ of total glacier runoff from
837 2002-2013, and made up most of the runoff from May through mid-July. Firn and ice melt
838 dominated runoff in August and September. Average September runoff exceeded that from June,
839 due to the large extent of exposed glacier ice this month. Contributions from ice and firn
840 constituted $42 \pm 14\%$ of the runoff and were highly variable, ranging from 19 to 62% over the
841 study period. Separation of meltwater derived from the seasonal snowpack and that from glacier
842 storage is important for long-term water resources planning, as the latter contribution is expected
843 to diminish as the century progresses (e.g., Stahl et al., 2008; Marshall et al., 2011).

On an annual basis, total glacier runoff (combined snow, firn and ice melt) made up 5-6% of the Bow River in Calgary from 2002-2013, with 2-3% coming from firn and ice. Runoff from glacier storage is concentrated in the period July through September, and exceeds 10% of the late-summer discharge of the Bow River in Calgary in hot, dry summers. Under drought conditions, when water demand is highest, runoff from glacier storage therefore provides an important late-summer supplement to the rivers on the eastern slopes of the Canadian Rocky Mountains. Glacier decline will reduce the efficacy of the natural reservoir function that has been historically provided by glaciers, and this should be accounted for in long-range water resource management planning in this region (Schindler and Donahue, 2006).

Caution is needed in extrapolating from observations at just one site, but the glaciological and hydroclimatic conditions at Haig Glacier are typical of continental, mid-latitude mountain regions. This study offers insight into the hydrological role of glaciers as landscape elements in such regions. Glaciers provide unusually high rates of specific discharge, concentrated late-summer release of meltwater, and an important supplement to streamflow under drought conditions. They also serve an interesting, largely unexplored, role as ‘snow traps’, augmenting the mountain snowpack. Reductions in summer snowmelt runoff due to glacier retreat would exacerbate the loss of meltwater derived from glacier storage in alpine regions.

Glacier runoff is the dominant component of mountain streams in glacierized catchments, but glacier contributions to streamflow will be limited at downstream sites for most mountain rivers as a result of the small fraction of the landscape covered by glaciers. Simple calculations based on the results presented here illustrate this well. Assuming that glaciers provide 10 times more specific discharge than other landscape elements in a basin, a catchment that is 1% glacierized

has 9% of its runoff originating from the glaciers. About 40% of this is derived from glacier storage during a period of strong glacier recession like the 2000s, giving 4% of the annual river discharge. This is well below the interannual variability in precipitation and discharge. It may also be negligible in the hydrological budget of major mountain rivers relative to uncertainties and possible increases in precipitation under future climate change (e.g., Immerzeel et al., 2013). Glaciers do matter for rivers draining from highly-glacierized catchments (e.g., more than 5% glacier cover) and for dry-season discharge in basins with limited upstream storage capacity.

ACKNOWLEDGEMENTS

I am indebted to the Natural Sciences and Engineering Research Council (NSERC) of Canada and the Canada Research Chairs program for support of longterm field studies at Haig Glacier. Tom Holland, Mike Norton, and the Canadian Olympic Development Association kindly tolerate us at their summer training facility on Haig Glacier. Steve Donelon, Melanie Percy, and Alberta Sustainable Resources Development have supported this research since its inception. Rick Smith at the University of Calgary Weather Research Station is instrumental in keeping the Haig Glacier weather stations ticking. It is odd to write a sole-authored article on Haig Glacier findings. This research has only been possible through the help of a host of students and friends too numerous to name who have contributed to the Haig Glacier effort since 2000.

REFERENCES

887 Adhikari, S. and Marshall S. J.: Influence of high-order mechanics on simulation of glacier
 888 response to climate change: insights from Haig Glacier, Canadian Rocky Mountains, *The*
 889 *Cryosphere*, 7, 1–15, doi:10.5194/tc-7-1-2013, 2013.

890 Alberta Environment: South Saskatchewan River Basin historical weekly natural flows, 1912–
 891 2001, v. 3.02, Environmental Monitoring and Evaluation Branch, Alberta Environment,
 892 Edmonton AB, 2004.

893 Arnold, N. S., Willis, I. C., Sharp, M. J., Richards, K. S. and Lawson, M. J.: A distributed
 894 surface energy-balance model for a small valley glacier. I. Development and testing for Haut
 895 Glacier d'Arolla, Valais, Switzerland, *J. Glaciol.*, 42 (140), 77-89, 1996.

896 Barnett T. P., Adam, J. C. and Lettenmaier, D. P.: Potential impacts of a warming climate on
 897 water availability in snow-dominated regions, *Nature*, 438, 303-309, 2005.

898 Bash, E. A. R. and Marshall, S. J.: Estimation of glacial melt contributions to the Bow River,
 899 Alberta, Canada, using a radiation-temperature melt model, *Ann. Glaciol.*, 55 (66), 138-152,
 900 2014.

901 Bolch, T., Menounos, B. and Wheate, R.: Landsat-based inventory of glaciers in western
 902 Canada, 1985-2005, *Remote Sensing of Environment*, 114, 127-137, 2010.

903 Braun, M. and Hock, R.: Spatially distributed surface energy balance and ablation modelling on
 904 the ice cap of King George Island (Antarctica), *Global and Planet. Change*, 42, 45-58, 2004.

905 BRBC: Bow River Basin Council, State of the Watershed Report, <http://wsow.brbc.ab.ca>, 2005.

906 Brock, B. W., Willis, I. C. and Sharp, M. J.: Measurement and parameterization of albedo
 907 variations at Haut Glacier d'Arolla, Switzerland, *J. Glaciol.*, 46 (155), 675-688, doi:
 908 10.3189/172756500781832675, 2000.

909 Coléou, C. and Lesaffre, B.: Irreducible water saturation in snow: experimental results in a cold
 910 laboratory. *Ann. Glaciol.*, 26, 64-68, 1998.

911 Comeau, L. E. L., Pietroniro, A. and Demuth, M. N.: Glacier contribution to the North and South
 912 Saskatchewan Rivers, *Hydrol. Processes*, 23, 2640-2653, 2009.

913 Demuth, M., Pinard, V., Pietroniro, A., Luckman, B., Hopkinson, C., Dornes, P. and Comeau,
 914 L.: Recent and past-century variations in the glacier resources of the Canadian Rocky
 915 Mountains: Nelson River system, In *Mountain glaciers and climate changes of the last*
 916 *century*, Bonardi, L. (Ed.), *Terra Glacialis*, 27-52, 2008.

917 Fountain, A. G. and Tangborn, W. V.: The effect of glaciers on streamflow variations, *Water*
 918 *Resour. Res.*, 21 (4), 579-586. 1985.

919 Grasby, S.E., Hutcheson, I. and McFarland, L.: Surface-water–groundwater interaction and the
 920 influence of ion exchange reactions on river chemistry, *Geology*, 27, 223–226, 1999.

921 Greuell, W. and Smeets, P.: Variations with elevation in the surface energy balance of the
 922 Pasterze (Austria), *J. Geophys. Res.*, 106 (D23), 31717-31727, 2001.

- 923 Hirose, J. M. R. and Marshall, S. J.: Glacier meltwater contributions and glacio-meteorological
924 regime of the Illecillewaet River Basin, British Columbia, Canada, *Atmosphere-Ocean*,
925 DOI:10.1080/07055900.2013.791614, 2013
- 926 Hock, R.: Glacier melt: a review of processes and their modelling, *Progress Phys. Geog.*, 29 (3),
927 362-391, 2005.
- 928 Hock, R. and Holmgren, B.: A distributed surface energy-balance model for complex topography
929 and its application to Storglaciären, Sweden, *J. Glaciol.*, 51 (172), 25-36, 2005.
- 930 Hopkinson, C. and Young, G. J.: The effect of glacier wastage on the flow of the Bow River at
931 Banff, Alberta, *Hydrol. Processes*, 12, 1745-1762, 1998.
- 932 Huss, M., Farinotti, D., Bauder, A. and Funk, M.: Modelling runoff from highly glacierized
933 alpine drainage basins in a changing climate, *Hydrol. Processes*, 22 (19), 3888–3902, doi:
934 10.1002/hyp.7055, 2008.
- 935 Huss, M.: Present and future contribution of glacier storage change to runoff from macroscale
936 drainage basins in Europe, *Water Resour. Res.*, 47, W07511, doi:10.1029/2010WR010299,
937 2011.
- 938 Immerzeel, W. W., Droogers, P., de Jong, S. M. and Bierkens, M. F. P.: Large-scale monitoring
939 of snow cover and runoff simulation in Himalayan river basins using remote sensing, *Remote*
940 *Sens. Environ.*, 113, 40-49, doi:10.1016/j.rse.2008.08.010, 2009.
- 941 Immerzeel, W.W., Pellicciotti, F. and Bierkens M. F.P.: Rising river flows throughout the
942 twenty-first century in two Himalayan glacierized watersheds. *Nature Geosci.*, 6, 742-745,
943 2013.
- 944 Jeelani, G., Feddema, J. J., van der Veen, C. J. and Stearns, L.: Role of snow and glacier melt in
945 controlling river hydrology in Liddar watershed (western Himalaya) under current and future
946 climate, *Water Resour. Res.*, 48, W12508, doi:10.1029/2011WR011590, 2012.
- 947 Klok, E. J. and Oerlemans, J.: Model study of the spatial distribution of the energy and mass
948 balance of Morteratschgletscher, Switzerland, *J. Glaciol.*, 48 (163), 505-518, 2002.
- 949 Lhomme, J. P., Vacher, J. J. and A. Rocheteau, A.: Estimating downward long-wave radiation on
950 the Andean Altiplano, *Agr. Forest Meteorol.*, 145, 139–148, 2007.
- 951 Marshall, S. J., Sharp, M. J., Burgess, D. O. and Anslow, F. S.: Near-surface temperature lapse
952 rate variability on the Prince of Wales Icefield, Ellesmere Island, Nunavut: Implications for
953 regional-scale temperature downscaling, *Int. J. Climatol.*, 27 (3), 385-398, 2007.
- 954 Marshall, S. J., White, E., Demuth, M., Bolch, T., Wheate, R., Menounos, B., Beedle, M., and
955 Shea, M.: Glacier water resources on the eastern slopes of the Canadian Rocky Mountains,
956 *Can. Water Resour. J.*, 36, 109–134, 2011.
- 957 Mark, B. G. and Seltzer, G. O.: Tropical glacier meltwater contributions to stream discharge: A
958 case study in the Cordillera Blanca, Peru, *J. Glaciol.*, 49, 271-281, 2003.
- 959 Meier, M. F., Dyurgerov, M. B., Rick, U. K., O’Neel, S., Pfeffer, W. T., Anderson, R. S.,
960 Anderson, S. P. and Glazovsky, A.F.: Glaciers dominate eustatic sea-level rise in the 21st
961 century, *Science*, 317, 1064-1067, 2007.

962 Moore, R. D. and Demuth, M. N.: Mass balance and streamflow variability at Place Glacier,
 963 Canada, in relation to recent climate fluctuations, *Hydrol. Processes*, 15, 3473-3486, 2001.

964 Moore, R. D., Fleming, S. W., Menounos, B., Wheate, R., Fountain, A., Stahl, K., Holm, K. and
 965 M. Jakob, M.: Glacier change in western North America: implications for hydrology,
 966 geomorphic hazards and water quality, *Hydrol. Processes*, 23, 42-61, 2009.

967 Munro, D.S.: Revisiting bulk heat transfer on the Peyto Glacier, Alberta, Canada, in light of the
 968 OG parameterization. *J. Glaciol.*, 50 (171), 590-600, 2004.

969 Nienow, P. W., Sharp, M. J. and Willis, I. C.: Seasonal changes in the morphology of the
 970 subglacial drainage system, Haut Glacier d'Arolla, Switzerland, *Earth Surf. Processes and*
 971 *Landforms*, 23, 825-843, 1998.

972 Oerlemans, J.: Analysis of a 3 year meteorological record from the ablation zone of
 973 Morteratschgletscher, energy and mass balance. *J. Glaciol.*, 46 (155), 571-579, 2000.

974 Oke, T. R.: *Boundary Layer Climates*, 2nd ed. Routledge, London, 1987.

975 Radić, V. and Hock, R.: Regionally differentiated contribution of mountain glaciers and ice caps
 976 to future sea-level rise, *Nature Geosci.*, doi:10.1038/NGEO1052, 2011.

977 Radić, V. and Hock, R.: Glaciers in the Earth's hydrological cycle: Assessments of glacier mass
 978 and runoff changes on global and regional scales. In *The Earth's Hydrological Cycle*,
 979 Springer, The Netherlands, pp. 813-837, 2014.

980 Rood, S. B., Samuelson, G. M., Weber, J. K. and Wywrot, K. A.: Twentieth century decline in
 981 streamflows from the hydrographic apex of North America, *J. Hydrol.*, 306, 215–233, 2005.

982 Schindler, D. W. and Donahue, W. F.: An impending water crisis in Canada's western prairie
 983 provinces, *Proc. Natl Acad. Sci. USA.*, 103 (19), 7210-7216, 2006.

984 Sedlar, J. and Hock, R.: Testing longwave radiation parameterizations under clear and overcast
 985 skies at Störglaciaren, Sweden, *The Cryosphere*, 3, 75-84, doi:10.5194/tc-3-75-2009, 2009.

986 Shea, J. M., Anslow, F. S. and Marshall, S. J.: Hydrometeorological relationships on the Haig
 987 Glacier, Alberta, Canada, *Ann. Glaciol.*, 40, 52-60, 2005.

988 Shea, J. M. and Marshall, S. J.: Synoptic controls on regional precipitation and glacier mass
 989 balance in the Canadian Rockies, *Int. J. Climatol.*, 27 (2), 233-247, 2007.

990 Sinclair, K. E. and Marshall, S. J.: The impact of vapour trajectory on the isotope signal of
 991 Canadian Rocky Mountain snowpacks, *J. Glaciol.*, 55 (191), 485-498, 2009.

992 Stahl, K., Moore, R. D., Shea, J. M., Hutchinson, D. G. and Cannon, A.: Coupled modeling of
 993 glacier and streamflow response to future climate scenarios, *Water Resour. Res.*, 44, W02422,
 994 doi:10.1029/2007WR005956, 2008.

995 WGMS: World Glacier Monitoring Service, Zurich, Switzerland. Glacier Mass Balance
 996 Bulletins (M. Zemp et al., Eds.), ICSU(WDS)/IUGG(IACS)/UNEP/UNESCO/WMO, data
 997 available at <http://wgms.ch/gmbb.html>, 2014.

998 Willis, I., Arnold, N. and Brock, B.: Effect of snowpack removal on energy balance, melt and
 999 runoff in a small supraglacial catchment, *Hydrol. Processes*, 16, 2721-2749, 2002.

1000 Wolfe B. B., Hall, R. I., Edwards, T. W. D., Jarvis, S. R., Sinnatamby, R. N., Yi, Y. and
1001 Johnston, J. W.: Climate-driven shifts in quantity and seasonality of river discharge over the
1002 past 1000 years from the hydrographic apex of North America, *Geophys. Res. Lett.*, 35, 1-5,
1003 2008.
1004

Tables

Table 1. Instrumentation at the glacier (G) and forefield (FF) AWS sites. Meteorological fields are measured each 10 seconds, with 30-minute averages archived to the dataloggers. Campbell Scientific dataloggers are used at each site, with a transition from CR10X to CR1000 loggers in summer 2007. Radiometers are both upward- and downward looking.

<i>Field</i>	<i>Instrument</i>	<i>Comments</i>
Temperature	HMP45-C	
Relative humidity	HMP45-C	
Wind speed/direction	RM Young 05103	
Shortwave radiation	Kipp & Zonen CM6B (FFAWS)	spectral range 0.35-2.50 μm
	Kipp and Zonen CNR1 (GAWS)	spectral range 0.305-2.80 μm
Longwave radiation	Kipp and Zonen CNR1 (GAWS)	spectral range 5-50 μm
Snow surface height	SR50 ultrasonic depth ranger	
Barometric pressure	Rm Young 61250V	

Table 2. Parameters in the distributed energy balance and melt model.

<i>Parameter</i>	<i>Symbol</i>	<i>Value</i>	<i>Units</i>
Glacier temperature offset	ΔT_d	-2.8	$^{\circ}\text{C}$
Glacier temperature lapse rate	β_T	-5.0	$^{\circ}\text{C km}^{-1}$
Specific humidity lapse rate	β_q	-1.1	$\text{g kg}^{-1} \text{ km}^{-1}$
Summer precipitation events	N_p	25	$^{\circ}\text{C m}^{-1}$
Summer daily precipitation	P_d	1-10	mm w.e.
Summer snow threshold	T_s	1.0	$^{\circ}\text{C}$
Summer fresh snow density	ρ_{pow}	145	kg m^{-3}
Snow albedo	α_s	0.4-0.86	
Firn albedo	α_f	0.4	
Ice albedo	α_i	0.25	
Snow albedo decay rate	k_α	-0.001	$(^{\circ}\text{C d})^{-1}$
Snow/ice roughness	z_0	0.001	m
Relation for ε_a (Eq. 5)	a_ε	0.407	
$[\varepsilon_a = a_\varepsilon + b_\varepsilon e_v/e_s + c_\varepsilon e_v]$	b_ε	0.60	
	c_ε	0.24	Pa^{-1}

Table 3. Mean value \pm one standard deviation of May snowpack data, based on snowpit measurements from sites at Haig Glacier, 2002-2013. Glacier-wide winter mass balance, B_w , is also reported. See Figure 1 for snow sampling locations.

<i>Site</i>	<i>z</i> (m)	<i>depth</i> (cm)	<i>SWE</i> (mm)	ρ_s (kg m ⁻³)
FFAWS	2340	174 \pm 62	770 \pm 310	400 \pm 70
mb02	2500	307 \pm 83	1365 \pm 370	445 \pm 40
mb10	2590	291 \pm 48	1210 \pm 240	415 \pm 35
GAWS	2665	304 \pm 44	1230 \pm 270	410 \pm 50
French Pass	2750	397 \pm 45	1700 \pm 320	420 \pm 50
Glacier (B_w)			1360 \pm 230	

Table 4. Mean monthly weather conditions at Haig Glacier, Canadian Rocky Mountains, 2002-2012, as recorded at an automatic weather station at 2665 m. N is the number of months with data in the 11-year record. Values are averaged over N months.

Month	T (°C)	T_{min} (°C)	T_{max} (°C)	PDD (°C d)	H (%)	e_v (mb)	q_v (g/kg)	P (mb)	v (m/s)	α_s	N
January	-11.8	-14.6	-8.9	1.6	73	1.9	1.7	738.5	4.1	0.88	5.0
February	-11.7	-14.8	-8.5	0.3	74	2.0	1.7	739.0	3.1	0.87	5.0
March	-10.9	-13.4	-7.9	1.2	78	2.3	2.0	738.3	3.1	0.89	5.5
April	-5.9	-9.6	-1.6	11.2	73	3.0	2.5	741.9	2.8	0.84	7.2
May	-1.6	-5.3	2.5	42.4	72	3.9	3.3	742.5	2.8	0.79	9.2
June	2.6	-0.4	6.2	96.3	71	5.1	4.4	747.2	2.6	0.73	10.0
July	6.6	3.3	10.1	217.0	62	5.9	5.0	750.8	2.8	0.59	9.8
August	5.8	2.6	9.4	183.8	64	5.7	5.0	750.3	2.5	0.41	9.9
September	1.5	-1.5	4.6	87.2	72	4.8	4.1	748.1	3.0	0.63	8.2
October	-3.8	-6.9	-0.9	23.1	69	3.3	2.8	744.4	3.7	0.76	4.9
November	-8.4	-11.1	-5.9	2.0	73	2.6	2.2	741.1	4.0	0.79	4.0
December	-12.8	-15.8	-10.2	0.2	74	1.9	1.6	739.0	3.9	0.81	3.9
JJA	5.0	1.8	8.6	497.1	66	5.6	4.8	749.4	2.6	0.55	9.7
Annual	-4.2	-7.3	-0.9	666.3	71	3.5	3.0	743.4	3.2	0.75	5.3

Table 5. Mean monthly surface energy balance at the Haig Glacier AWS, 2002-2012. Radiation fluxes are measured. Turbulent and conductive heat fluxes are modeled. All fluxes are in W m^{-2} except for the monthly melt energy Q_m , in MJ m^{-2} . Melt is the total monthly melt (mm w.e.).

Month	Q_s^\downarrow	Q_s^\uparrow	Q_L^\downarrow	Q_L^\uparrow	Q^*	Q_H	Q_E	Q_G	Q_N	Q_m	melt (mm)
January	47	37	225	251	-17	-34	-26	0.5	-76	0	0
February	101	77	215	251	-12	-25	-20	0.4	-57	0	0
March	137	115	225	250	-2	-14	-14	0.2	-29	0	0
April	200	165	243	276	2	-9	-17	-0.6	-25	0	0
May	228	177	259	294	16	1	-15	-0.7	1	17	52
June	223	155	278	306	39	14	-8	0.2	46	119	355
July	220	122	280	312	66	35	0	0.1	101	271	808
August	187	76	276	311	83	27	-1	0.3	109	292	871
September	123	83	267	302	12	10	-12	0.9	11	49	148
October	91	67	247	282	-11	-7	-22	1.5	-39	~0	0
November	49	38	234	259	-14	-24	-21	1.9	-57	0	0
December	32	25	226	245	-13	-34	-23	1.3	-69	0	0
JJA	210	115	278	310	63	25	-3	0.2	85	682	2034
Annual	136	94	248	278	12	-5	-15	0.5	-3	748	2234

Table 6. Modeled surface mass balance and summer (JJA) surface energy balance at Haig Glacier, 2002-2013. B_w is winter (October to May) snow accumulation; B_{ws} is the summer snow accumulation; B_s is summer (May to September) ablation, and B_a is the annual (net) surface mass balance. Energy fluxes are in W m^{-2} , mass balances are mean specific values (mm w.e.), T_{JJA} is the mean glacier JJA temperature ($^{\circ}\text{C}$) and PDD is May-September positive degree days ($^{\circ}\text{C d}$).

Year	B_w	B_{ws}	B_s	B_a	Q_s^{\downarrow}	α	Q_L^{net}	Q^*	Q_H	Q_E	Q_N	T_{JJA}	PDD
2002	1770	68	2210	-370	181	0.58	-19	57	27	-3	81	5.1	601
2003	1130	57	2580	-1400	223	0.54	-35	68	31	-7	93	6.5	733
2004	1160	59	1780	-550	176	0.59	-27	44	22	-0	65	4.9	542
2005	1150	55	2160	-960	191	0.57	-20	61	24	-4	81	4.3	505
2006	1350	35	3690	-2300	207	0.49	-18	87	31	4	123	6.0	754
2007	1630	53	2320	-640	209	0.57	-35	55	31	-5	82	5.7	645
2008	1390	72	1940	-480	192	0.62	-27	47	22	-8	61	4.2	505
2009	1240	35	2190	-910	199	0.58	-36	48	23	-6	65	5.0	696
2010	1080	66	1490	-340	192	0.63	-34	37	21	-7	51	4.2	498
2011	1340	39	2240	-850	218	0.59	-29	59	21	-9	72	4.1	605
2012	1690	37	2590	-880	210	0.58	-25	64	26	-5	84	5.1	703
2013	1370	41	3070	-1670	189	0.55	-9	75	28	2	105	4.9	636
Mean	1360	51	2350	-960	199	0.58	-26	58	26	-4	81	5.0	619
StdDev	230	14	590	580	15	0.04	8	14	4	4	20	0.8	92

Table 7. Mean (\pm standard deviation) of modeled monthly meltwater runoff at Haig Glacier, 2002-2013, expressed as areally-averaged specific snow and ice melt on the glacier (mm w.e.). f_{ice} is the fraction of meltwater runoff derived from melting of glacier ice or firn.

	May	June	July	August	Sept.	Annual
snow melt	70 ± 50	270 ± 120	670 ± 170	330 ± 210	30 ± 20	1370 ± 230
ice melt	—	—	100 ± 180	540 ± 290	340 ± 190	980 ± 560
total melt	70 ± 50	270 ± 120	770 ± 260	870 ± 140	370 ± 190	2350 ± 590
f_{ice}	0.0	0.0	0.13	0.62	0.92	0.42 ± 0.14

Meltwater Runoff from Haig Glacier, Canadian Rocky Mountains, 2002-2013

Figure 1. Haig Glacier, Canadian Rocky Mountains, indicating the location of the automatic weather stations (GAWS, FFAWS), additional snowpit sites (mb02, mb10 and French Pass), the mass balance transect (red/blue circles), the Veriteq T/h stations, and the forefield stream gauge. Inset (a) shows the location of the study site, and inset (b) provides more regional perspective, including the municipalities of Calgary and Banff, Alberta.

Figure 2. Mean daily weather at Haig Glacier, 2002-2012. Black and red lines are GAWS and FFAWS data, respectively. (a) Temperature, $^{\circ}\text{C}$. The turquoise line indicates the glacier temperature derived from the FFAWS data. (b) Specific humidity, g kg^{-1} . (c) Wind speed, m s^{-1} . (d) Radiation fields at the GAWS, W m^{-2} . From top to bottom: outgoing longwave (red), incoming longwave (blue), incoming shortwave (black) and outgoing shortwave (orange).

Figure 3. Mean monthly temperatures at Haig Glacier, 2002-2012. (a) GAWS (blue), FFAWS (red), and derived glacier means (black). (b) Temperature differences, GAWS–FFAWS (blue, scale at right, $^{\circ}\text{C}$) and as a ‘lapse rate’ (brown, scale at left, $^{\circ}\text{C km}^{-1}$).

Figure 4. Mean daily (a) shortwave radiation fluxes, W m^{-2} , and (b) albedo evolution at the GAWS and FFAWS sites for the period April 1 to October 31, 2002-2012. Black (GAWS) and red (FFAWS) indicate incoming radiation and purple (GAWS) and brown (FFAWS) indicate the reflected/outgoing radiation and the mean daily albedo.

Figure 5. Mean monthly surface energy fluxes (W m^{-2}) and melt rates (mm w.e. d^{-1}) at the glacier AWS, 2002-2012. (a) Net radiation, Q^* (black), and sensible heat flux, Q_H (red). (b) Net energy, Q_N (grey), daily melt rates (yellow line), and average monthly melt rates (orange line).

Figure 6. Modeled (a) summer melt and (b) net mass balance vs. elevation (mm w.e.) at Haig Glacier, summer 2012.

Figure 7. Measured vs. modeled (a) melt and (b) net energy balance at the GAWS, 2002-2012. Melt observations are plotted for a range of time intervals for which we have direct snowpit or ablation stake data. Net energy balance values are daily for all years (May through Sept). One-to-one lines are plotted in each graph.

Figure 8. Daily and cumulative runoff from Haig Glacier, May 1-Sept 30, based on average daily values from 2002-2013. (a) Snowmelt (red), ice and firn melt (blue), and total melt (black), mm w.e. d^{-1} . (b) Cumulative snow, ice/firn, and total meltwater, along with the mean glacier snowpack (green), mm w.e. All values are glacier-averaged.

Figure 9. Measured discharge in Haig Stream, July 24-September 22, 2013 ($\text{m}^3 \text{s}^{-1}$). The green line indicates 15-minute data and the heavy blue line is the mean daily discharge.

Figure 10. Discharge in Haig Stream (blue, $\text{m}^3 \text{s}^{-1}$) and modeled glacier melt rates (red, mm w.e. h^{-1}), September 7-14, 2013.

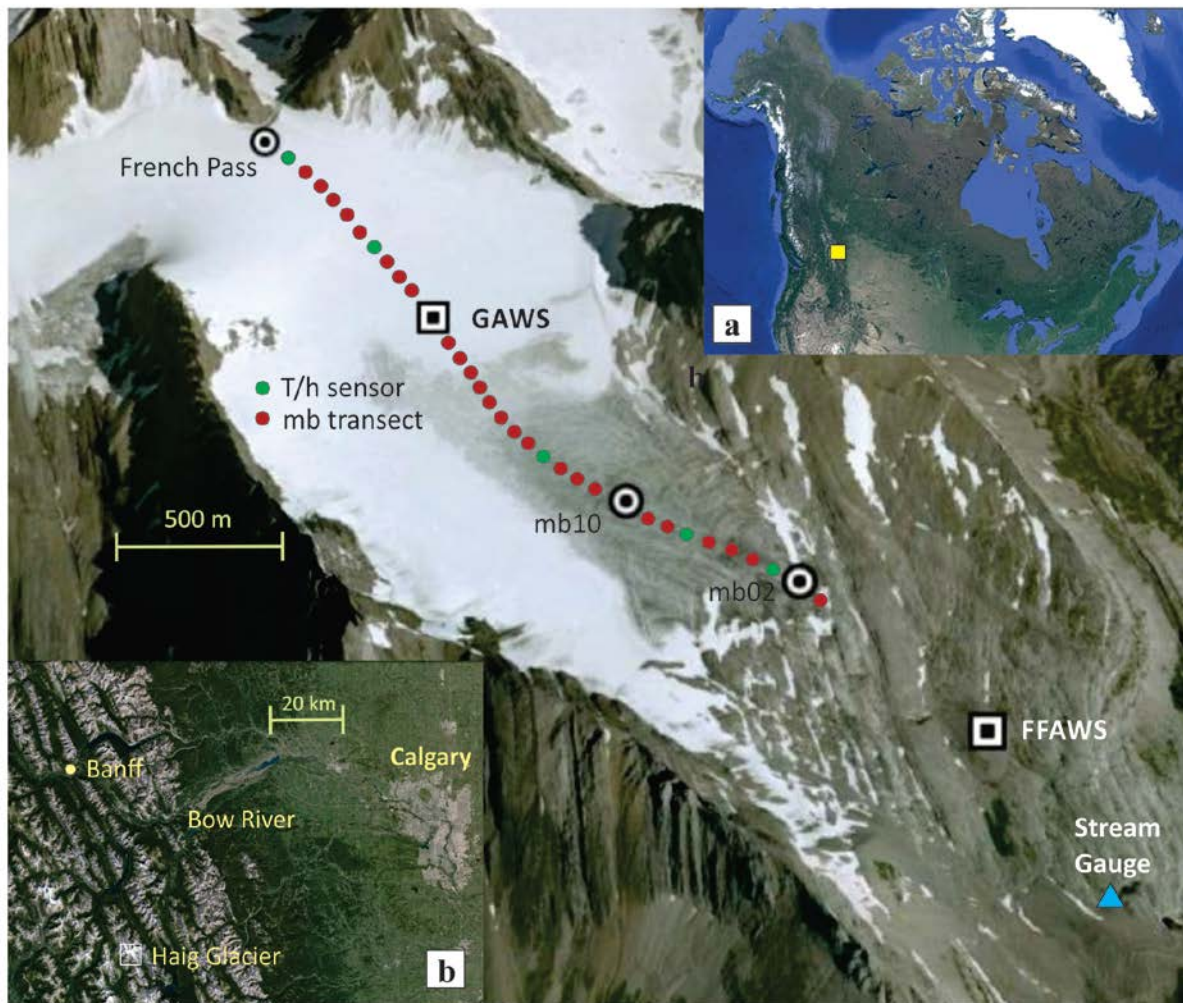


Figure 1. Haig Glacier, Canadian Rocky Mountains, indicating the location of the automatic weather stations (GAWS, FFAWS), additional snowpit sites (mb02, mb10 and French Pass), the mass balance transect (red/blue circles), the Veriteq T/h stations, and the forefield stream gauge. Inset (a) shows the location of the study site, and inset (b) provides more regional perspective, including the municipalities of Calgary and Banff, Alberta.

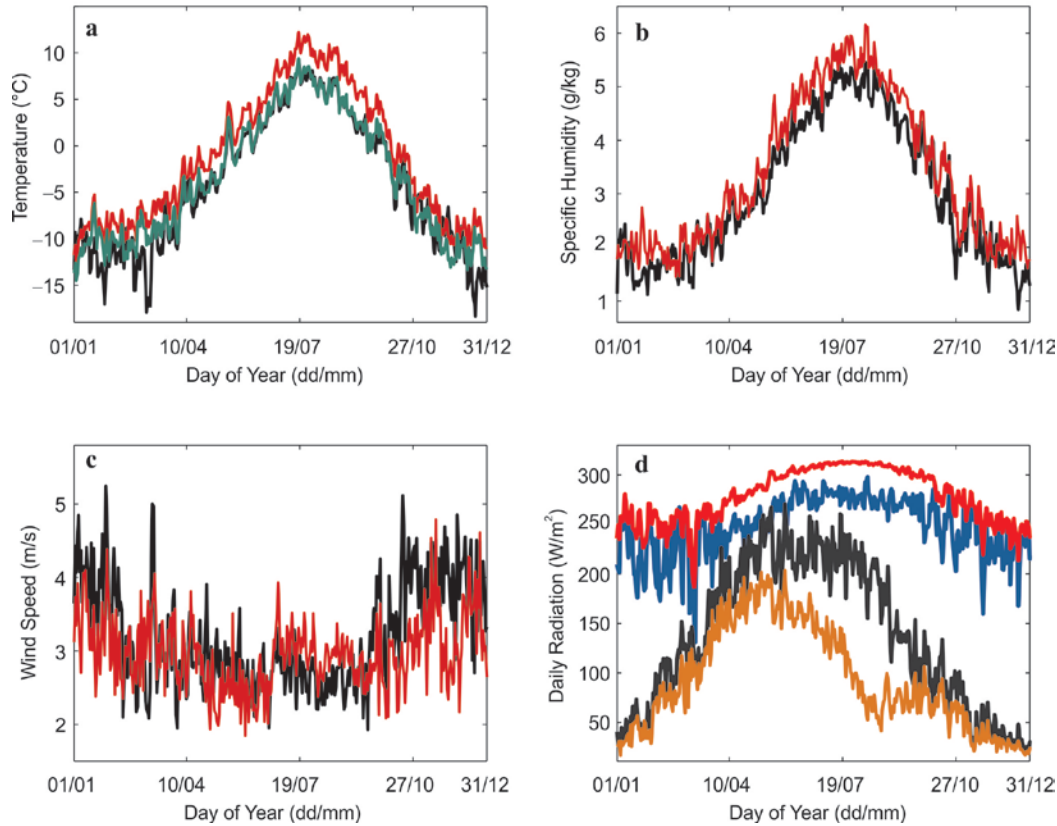


Figure 2. Mean daily weather at Haig Glacier, 2002-2012. Black and red lines are GAWS and FFAWS data, respectively. (a) Temperature, °C. The turquoise line indicates the glacier temperature derived from the FFAWS data. (b) Specific humidity, g kg^{-1} . (c) Wind speed, m s^{-1} . (d) Radiation fields at the GAWS, W m^{-2} . From top to bottom: outgoing longwave (red), incoming longwave (blue), incoming shortwave (black) and outgoing shortwave (orange).

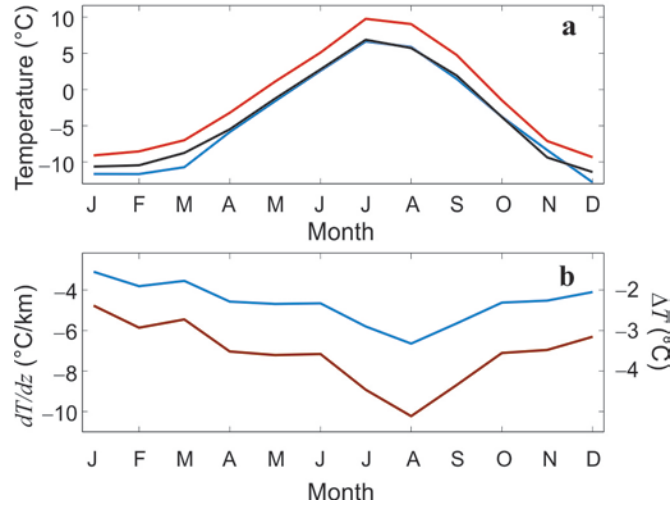


Figure 3. Mean monthly temperatures at Haig Glacier, 2002-2012. (a) GAWS (blue), FFAWS (red), and derived glacier means (black). (b) Temperature differences, GAWS–FFAWS (blue, scale at right, °C) and as a ‘lapse rate’ (brown, scale at left, °C km⁻¹).

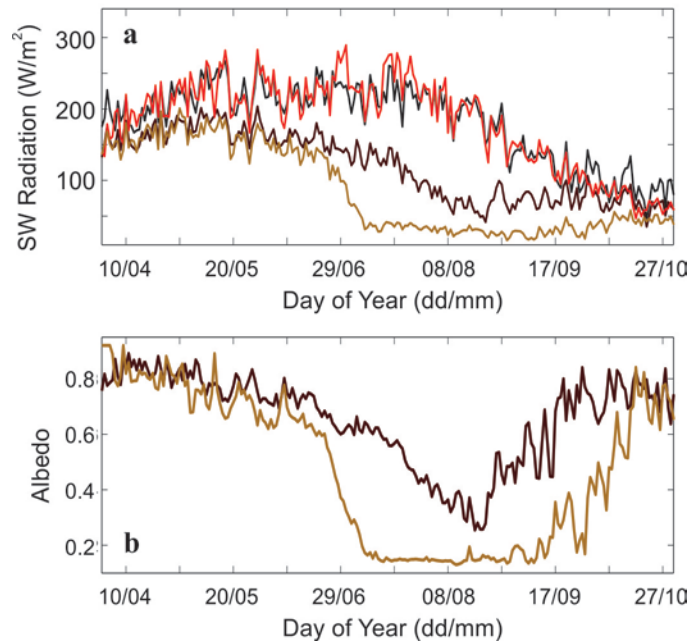


Figure 4. Mean daily (a) shortwave radiation fluxes, W m⁻², and (b) albedo evolution at the GAWS and FFAWS sites for the period April 1 to October 31, 2002-2012. Black (GAWS) and red (FFAWS) indicate incoming radiation and purple (GAWS) and brown (FFAWS) indicate the reflected/outgoing radiation and the mean daily albedo.

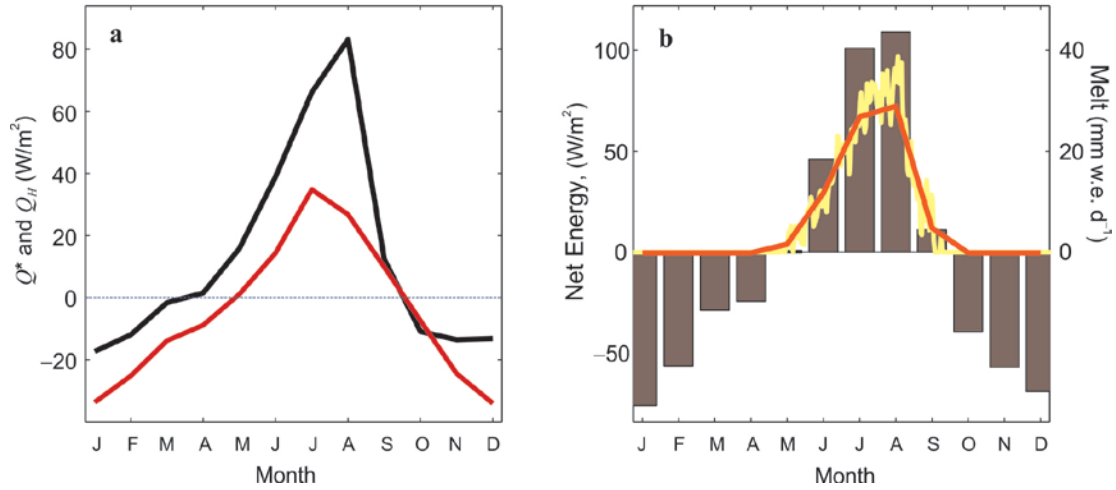


Figure 5. Mean monthly surface energy fluxes (W m^{-2}) and melt rates (mm w.e. d^{-1}) at the glacier AWS, 2002-2012. (a) Net radiation, Q^* (black), and sensible heat flux, Q_H (red). (b) Net energy, Q_N (grey), daily melt rates (yellow line), and average monthly melt rates (orange line).

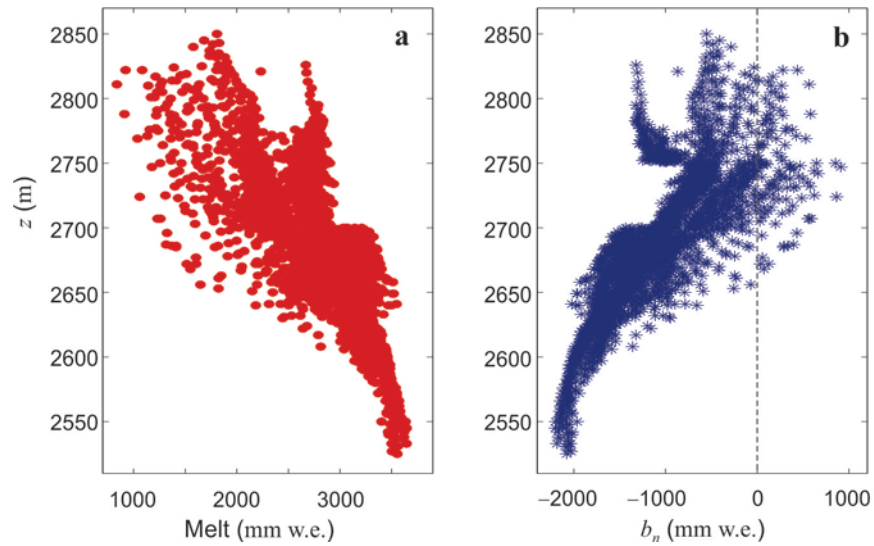


Figure 6. Modeled (a) summer melt and (b) net mass balance vs. elevation (mm w.e.) at Haig Glacier, summer 2012.

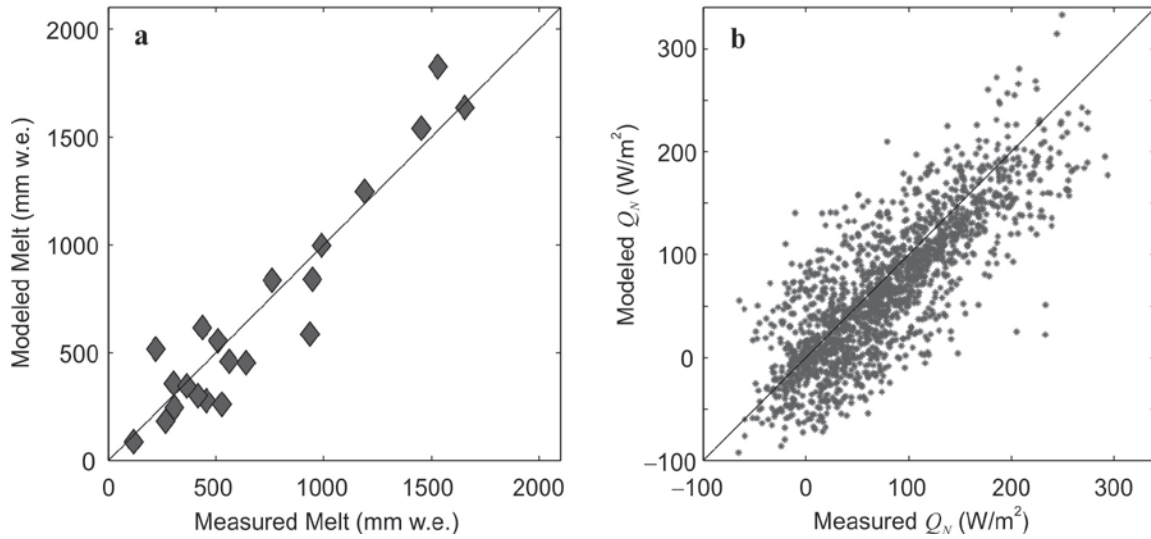


Figure 7. Measured vs. modeled (a) melt and (b) net energy balance at the GAWS, 2002-2012. Melt observations are plotted for a range of time intervals for which we have direct snowpit or ablation stake data. Net energy balance values are daily for all years (May through Sept). One-to-one lines are plotted in each graph.

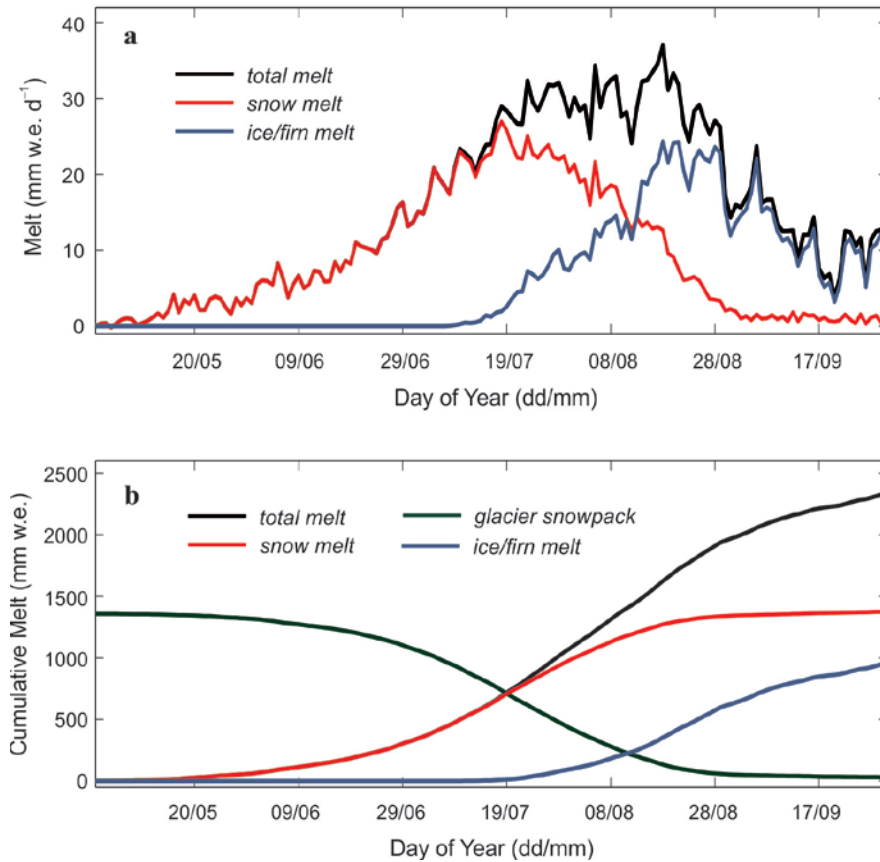


Figure 8. Daily and cumulative runoff from Haig Glacier, May 1-Sept 30, based on average daily values from 2002-2013. (a) Snowmelt (red), ice and firn melt (blue), and total melt (black), mm w.e. d⁻¹. (b) Cumulative snow, ice/firn, and total meltwater, along with the mean glacier snowpack (green), mm w.e. All values are glacier-averaged.

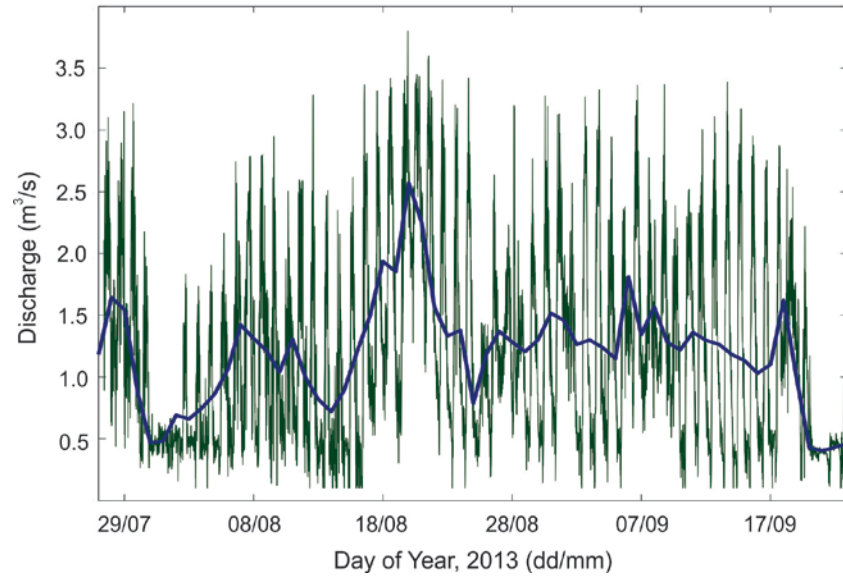


Figure 9. Measured discharge in Haig Stream, July 24-September 27, 2013 ($\text{m}^3 \text{s}^{-1}$). The green line indicates 15-minute data and the heavy blue line is the mean daily discharge.

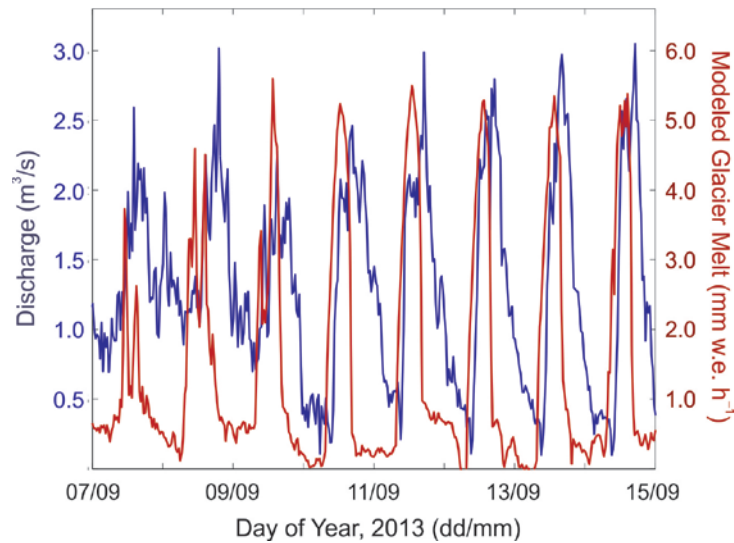


Figure 10. Discharge in Haig Stream (blue, $\text{m}^3 \text{s}^{-1}$) and modeled glacier melt rates (red, mm w.e. h^{-1}), September 7-14, 2013.